substituting Eq. (2.41) into Eq. (2.40), switching the order of integration, and then invoking the delta function formula

$$\delta(x)=(2\pi)^{-1}\int_{-\infty}^{\infty} e^{i\omega x}\,d\omega=2\int_{0}^{\infty}\cos(2\pi\nu x)d\nu.$$

[18]A rigorous derivation of the widely known formulas (2.48), which is sometimes called the Box–Muller algorithm, may be found in Ref. 10, Sec. 1.8, which also describes a simple procedure for generating values for $r_1$ and $r_2$ in Eqs. (2.48a).

[19]It is possible to construct a simulation algorithm for O–U processes that is exact for *both* $Y$ and $X$, but to do that we need a little more random variable theory than is given in Sec. II B.

[20]A nice account of Einstein's work in Ref. 1 is given in Ref. 9, pp. 2–6.

[21]D. T. Gillespie, "Fluctuation and dissipation in Brownian motion," Am. J. Phys. **61**, 1077–1083 (1993). A more sophisticated argument is given in Ref. 10, Secs. 4.5 and 4.6.

[22]Nyquist's original analysis in Ref. 5 proceeds quite differently from the analysis that we give here; see Ref. 7, p. 592.

[23]J. R. Reitz and F. J. Milford, *Foundations of Electromagnetic Theory* (Addison-Wesley, Reading, MA, 1960), p. 176.

[24]See, e.g., Ref. 7, Sec. 7.5.

[25]A short proof of this "lemma" may be found in Ref. 10, p. 114.

# Photon counting statistics—Undergraduate experiment

P. Koczyk, P. Wiewiór, and C. Radzewicz
*Institute of Experimental Physics, Warsaw University, ul. Hoża 69, 00-681 Warsaw, Poland*

(Received 3 May 1995; accepted 19 July 1995)

A photon counting experiment for student physics laboratory is described. It is designed to illustrate the probabilistic nature of the photodetection process itself as well as statistical fluctuations of light. The setup enables the student to measure photon count distributions for both coherent and pseudothermal light sources yielding Poisson and Bose–Einstein distributions, respectively.


## I. INTRODUCTION

Photon counting is a technique commonly used to measure extremely low light fluxes. A photomultiplier tube (PMT) of proper design is used to convert light into an electrical signal. (The most important property of photon counting PMT is very high gain at the first dynode. This allows one to distinguish between the pulse[1] resulting from electrons ejected from the photocathode and those coming from the dynodes.) Light impinging on the photocathode of the PMT ejects electrons from it. Assuming that the gain of the PMT itself and that of the following electronics is high enough, one can distinguish individual electrical pulses, each of them corresponding to a single photoelectron. The electrical pulses from the PMT are fed into a discriminator and pulses with amplitudes higher than a given threshold value are counted. Those are usually referred to as photon counts. This way one can count the number of electrical pulses, ideally each of them corresponding to a single photoelectron. Since for each photoelectron created one photon of the light field has to be destroyed, the method is commonly called photon counting. Thus, in this oversimplified picture, one can think of the method as a way to prove the existence of photons. This is not true. Actually there is no need to quantize the electromagnetic field in order to explain all the features of the photoelectric process. All that is necessary is an assumption that the light interacts with matter which is described quantum mechanically. This leads to what is commonly referred to as a semiclassical description,[2] a model in which light is described as a classical electromagnetic wave and the atomic system, the photocathode in our case, quantum mechanically. The question of whether one has to invoke the quantum nature of electromagnetic field at all has been disputed ever since Einstein introduced the notion of the "light quantum" in 1905 in his paper describing the external photoelectric process.[3] Several different models for the photon have been proposed starting with a simple particle model and ending with what is known as Dirac's model,[4] each of them presenting its own difficulties in interpretation. Amazingly enough, the answer to this question has been settled quite recently when experiments on photon antibunching[5] and squeezed states (for a review on the topic see, for example, the paper by Walls[1]) proved that at least in some cases a quantum mechanical description of the light is necessary. Since in the experiments described in this paper the light can be perfectly described in a classical way, the semiclassical picture will be used henceforth.

The noise present in photon counting can be separated into two terms. The first is of a technical nature and is caused predominantly by electrical pulses created by amplification of electrons thermally released from the photocathode or the first dynode, which cannot be distinguished from the pulses corresponding to photoelectrons. Those pulses are present even if there is no light falling on the photocathode and for this reason are called dark counts. The dark count rate can be minimized by proper design and cooling of the PMT. Currently, even modestly priced systems have a dark count rate as small as a few counts per second. We will assume throughout this paper that the dark counts can be neglected altogether. The second contribution to the noise in the photon counting experiment and the only one considered in this paper is of a fundamental nature and cannot be eliminated. Again, it can be divided into two parts caused by the stochastic nature of photoelectric process and light intensity fluctuations, respectively. Using the semiclassical model mentioned above one finds that for a constant intensity of light reaching

  

the photocathode the photoelectrons tend to leave the photocathode at random times. Thus the number of photon counts in a given time interval is not constant. Instead it fluctuates, leading to noise which is often referred to as shot noise. It is a fundamental feature of the photoelectric process. On the one hand, one can think that the photocurrent from the photocathode is constant but is formed by a discrete flow of electrons. Then the shot noise in the PMT tube is of the same nature as the shot noise in any vacuum tube. On the other hand one can think of each of the photoelectrons as being ejected as a result of absorption and destruction of one photon from the light beam. In this picture the statistics of photon counts reflects the statistics of photons in the measured light beam. It is important to stress that the shot noise will be present in photon counting experiments whenever the radiation measured can be described classically. However, for squeezed states a subshot noise operation of the photon counting PMT is possible.[6] Turning back to a semiclassical description, in addition to the shot noise, extra fluctuations in the photon count number arise whenever the intensity of the light being measured is not constant. In this case the photon counting statistics depend on the experimental details and reveal both the random nature of the photoelectric process itself and the nature of light fluctuations.

## II. PHOTON COUNTING STATISTICS

The elementary experiment in photon counting is one in which photoelectrons are counted during a given time interval $T$. Since, as we have already mentioned in the Introduction, the photoelectric process is stochastic, one should expect that the number of photon counts will be stochastic, too. This means that the outcome of such an experiment cannot be predicted in advance. The most one can know is the probability of obtaining any given result. The formula for this probability distribution was first derived in the late 1950s by Mandel.[7] Before writing Mandel's formula explicitly, let us define the integrated light intensity $W$ as[8]

$$W=\int\int_{A}\int_{t}^{t+T} I(x,y;\xi)\,d\xi\,dx\,dy, \tag{1}$$

where $I(x,y;\xi)$ is the intensity of the light wave at point $(x,y)$ and time $\xi$, and $A$ is the illuminated area of the photocathode. As defined by formula (1), $W$ is the energy of the light beam reaching the photocathode during a time interval starting at $t$ and ending at $t+T$. In general, $W$ is a stochastic variable with a probability density function given by $P_W(W)$. The probability of observing $K$ photon counts during time interval $T$ is given by Mandel's formula[7]

$$P(K)=\int_0^{\infty}\frac{(\alpha W)^K}{K!}\exp(-\alpha W)P_W(W)\,dW, \tag{2}$$

where $\alpha=\eta/h\nu$ and $\eta$ is the quantum efficiency of the photocathode, $h$ is Planck's constant, and $\nu$ is the light frequency. As should be expected, the number of photon counts recorded in the time interval $T$ is proportional to the energy delivered by the light beam to the photocathode during this time interval. Thus, in general, any fluctuations in the light intensity will, in principle, lead to fluctuations in the recorded number of photon counts. However, even for the light beam with perfectly constant intensity the number of the photon counts recorded during time $T$ is not constant. This can be easily seen by performing the integration in formula (2) with an assumption

$$P(W)=\delta(W-\bar{W}),$$

where $\bar{W}$ is the average (constant) integrated intensity. The result of the integration is the Poisson distribution

$$P(K)=\frac{\bar{K}^K}{K!}\exp(-\bar{K}), \tag{3}$$

with the average number of photon counts $\bar{K}=\alpha\bar{W}$. Therefore, even in the photon counting experiment with a constant intensity light source, one observes stochastic variations in the number of counts. The resulting noise is the shot noise.

Two distinct light sources are of particular interest. The first one is a single-mode laser operating well above the threshold. The light emitted by such a laser is classically described by a constant amplitude perfectly monochromatic wave. Obviously the intensity of such a light beam is constant. Therefore, in this case, one should expect that the photon count distribution will be given by the Poisson distribution (3). It is worth mentioning that the quantum mechanical description of the light from a single-mode laser uses a coherent state mode[9] which converges to the classical description in the high-intensity limit.[10] The second light source of interest is a thermal source, i.e., a discharge lamp, incandescent lamp, etc. It is easy to see why the intensity of light from such a source is not constant. In this case the light field is a superposition of many waves with random amplitudes and phases being emitted by individual atoms or molecules in the discharge. It is very useful to introduce the notion of the coherence time for such field. We will not do it rigorously here; instead, we will define the coherence time heuristically. One can think of an amplitude and phase of the thermal light as changing stochastically but with a finite rate. This means that given the knowledge of the amplitude and phase at any given moment of time, one can with some accuracy predict what these parameters will be some short time later. On the other hand, after a long enough time, the field amplitude and phase are not correlated with their initial values and one cannot make any predictions. Thus one can say that the field "remembers" its previous parameters over some characteristic time. This time is called the coherence time. It is inversely proportional to the spectral width of the light source and for true thermal sources such as an incandescent lamp is very short. The instantaneous intensity probability density function for a linearly polarized thermal field is a negative exponential with zero intensity being the most probable:

$$P(I)=\frac{1}{\bar{I}}\exp\left(-\frac{I}{\bar{I}}\right), \tag{4}$$

where $\bar{I}$ is the average intensity.

For thermal light the integrated intensity probability density $P_W(W)$ depends on the time interval used. Two limiting cases are easy to analyze. For $T$ much shorter than the coherence time $\tau_c$, the integrated intensity $W$ has the same distribution as the instantaneous intensity [formula (4)] and the photon count distribution is given by the Bose–Einstein formula:

$$P(K)=\frac{1}{1+\bar{K}}\left(\frac{\bar{K}}{1+\bar{K}}\right)^K \tag{5}$$

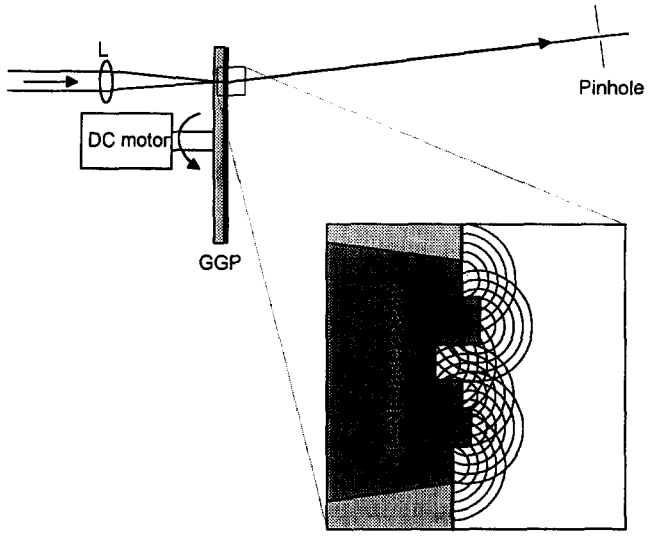


Fig. 1. Principle of pseudothermal light generation. L is a lens and GGP is a ground-glass plate. The laser beam is focused on the ground surface of the plate and the scattered light observed behind the pinhole P. The inset shows schematically a magnified part of the plate with several areas of various thicknesses illuminated by the laser beam. Sets of concentric circles indicate that each of the elementary areas is a source of a spherical wave.

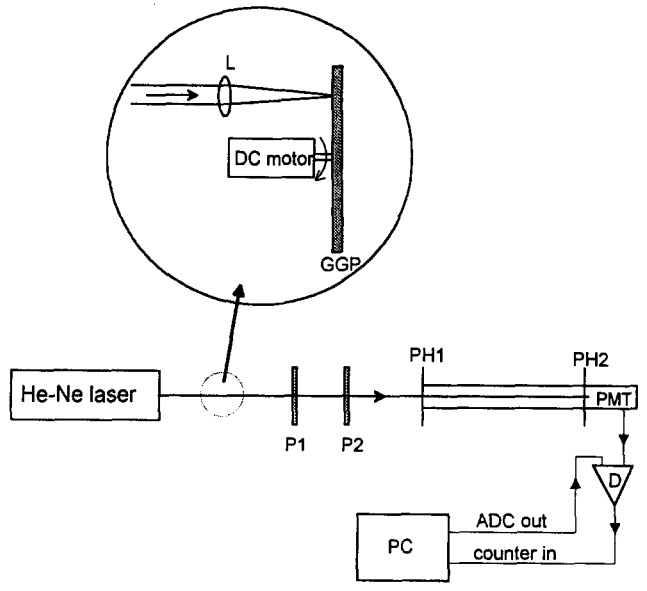


Fig. 2. Experimental setup P1, P2—Polaroid polarizers; PH1 and PH2—pinholes; PMT—photon counting photomultiplier tube; D—discriminator; PC—personal computer. The inset shows a ground-glass plate (GGP) mounted on a dc motor, and a lens (L) which were optionally inserted into the laser beam in order to produce pseudothermal light.

while for $T \gg \tau_c$ the function $P_W(W)$ is constant, the same as for a single-mode laser. Unfortunately, the coherence time for true thermal sources is very short (usually shorter than 1 ps) and for technical reasons one cannot measure $P(K)$ for $T \ll \tau_c$. However, one can easily make a pseudothermal light from the laser light. This can be achieved by scattering laser light from a large set of moving, randomly distributed scattering centers. Two methods for achieving this have been reported as early as the 1960s. The first one relies on scattering the light from a collection of submicron-sized plastic balls suspended in liquid,[11] while the second uses a rotating ground-glass plate.[12] The latter was used in our experiment. The principle of generating pseudothermal light using this method is illustrated in Fig. 1. Each of the elementary areas on the uneven glass surface illuminated by the laser beam forms a source of a spherical wave as illustrated in the inset. The optical field observed in the position of the pinhole is a sum of many waves with amplitudes and phases determined, respectively, by the size and relative positions of the respective scattering areas. Since both size and position of these areas are random, the resulting field is composed of many components with random amplitudes and phases. The resulting light intensity varies dramatically with the position of the observation point. This leads to a well-known phenomenon called speckle. If the glass plate is translated perpendicularly to the beam the speckle pattern changes and the light field observed behind the pinhole fluctuates. It can be shown that for the aperture diameter much smaller than speckle grain size, the intensity of light behind the aperture displays fluctuations described by the same formula as those of the thermal light.[11] The advantage of using this method to produce pseudothermal light is that one can easily control the correlation time of the fluctuating light produced this way. It can be continuously adjusted by changing the speed with which the glass moves across the laser beam. Light scattered from the ground-glass plate at some angle to the beam axis was used in our experiment to imitate a thermal source.

## III. EXPERIMENT

The experimental setup is shown in Fig. 2. A 5-mW polarized He–Ne laser was used as a light source throughout the measurements. The laser beam passed through two Polaroid polarizers P1 and P2, and two pinholes, PH1 and PH2, mounted at the ends of a black metal tube of about 0.5-m length before reaching the photon counting PMT. The purpose of the pinholes and the metal tube is to decrease the solid angle viewed from the photocathode of the PMT and thus limit as far as possible the amount of the stray light reaching the photocathode. At the same time by appropriate choice of the pinhole diameters the intensity of the laser light impinging on the photocathode can be brought to a reasonably low level of about few thousand counts per second. The pinholes were made by carefully piercing holes in aluminum foil with a sharp needle. The pinhole diameters used were from about 50 $\mu$m to about 200 $\mu$m as measured from the diffraction pattern of the laser beam. Final adjustment of the light intensity and thus the photoelectron count rate was made by rotating the second polarizer. To produce pseudothermal light a 10-cm focal length lens and a slowly rotating ground glass disk were inserted into the laser beam as shown schematically in the picture. A dc motor was used to turn the glass. A photodiode with a small active area was temporarily set in the position of the first pinhole and the signal from the photodiode observed on an oscilloscope. This enabled us to adjust the motor speed in such a way that the intensity fluctuations observed on the scope had a characteristic time of about 100 ms. This gave us an order of magnitude estimate for the coherence time $\tau_c$ of the light. It should be much longer than the photon counting time interval $T$ (in our case 1 ms) if the Bose–Einstein distribution is to be observed. The PMT used was a Hamamatsu H4730-01 photon counting head consisting of the PMT tube itself as well as an amplifier and a discriminator. The discriminator produced a transistor–transistor logic (TTL) level pulse whenever the output pulse from the PMT tube had an amplitude higher than a given

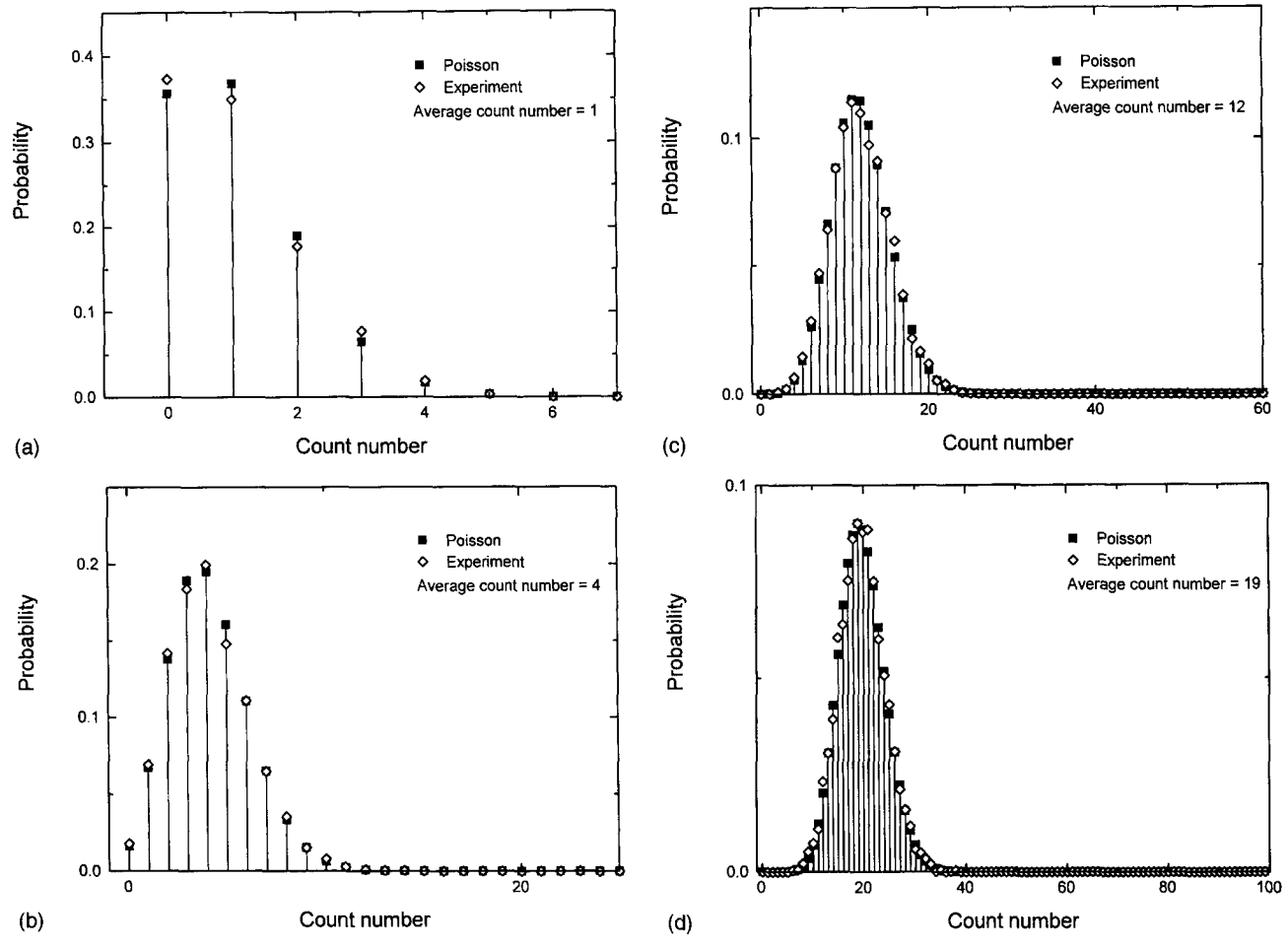


Fig. 3. Experimental photon count distributions (diamonds) measured for the He–Ne laser light and Poisson distributions (squares) with corresponding average values. (a)–(d) Results for count numbers 1, 4, 12, and 19, respectively.

threshold value. The TTL pulses were fed into a pulse counter board (Advantech model PCL-720) in a IBM compatible PC computer. Another plug-in board in the computer was used to provide an analog output voltage which determined the discriminator threshold. A rather straightforward computer code was written to control the DA converter and the counter boards. The code enabled the following tasks to be performed by the computer: setting the discriminator threshold, repetitive photon counting over a given time interval $T$, calculating average count number $\bar{K}$ and probability distribution.

First, the characteristics of the photon counting system itself were measured. With the PMT supply voltage set at +1000 V, a distribution function of the PMT pulse amplitude $K(V_d)$ was measured by varying the discriminator threshold between −0.5 and −2.5 V. Numerical differentiation of $K(V_d)$ yielded the PMT pulse amplitude probability density function. This function showed a rather weakly pronounced single-photon peak centered around −1.5 V. The result confirmed the manufacturer's recommendation for a −1.0 V discriminator threshold and this value has been used in all the following measurements. In order to measure the dark count rate, the input of the PMT was blocked and an average of 100 measurements each lasting 1 s was taken for different values of PMT supply voltage. The results obtained showed that the dark count rate increases monotonically with the PMT high voltage in the range of +800 to +1200 V. For a PMT high voltage of +1000 V, the dark count rate was about 60 counts/s which is slightly lower than specified for this instrument. All the following measurements were carried out in such a way as to make the contribution of the dark counts insignificant. For example, if the average count number $\bar{K}$ desired was 5, then the counting time $T$ was chosen to be 1 ms and thus average dark count rate during time $T$ was 0.06 which is negligible compared to $\bar{K}$. For higher values of $\bar{K}$ the counting time $T$ could be appropriately extended while keeping the dark count contribution at the negligible level.

Photon count distributions were measured for both He–Ne laser light and pseudothermal light produced by a rotating disk of ground glass as described before. In each of the measurements the procedure was as follows. First, the average count rate was adjusted to the desired value by changing the light intensity with the polarizer P2. Then a series of 10 000 measurements was taken and the data stored in computer memory. Finally, the probability distribution was calculated as the ratio of the number of measurements with a given number of counts to the total number of measurements. The time interval $T$ used varied from 1 to 10 ms, but all the measurements for the pseudothermal light were taken with $T=1$ ms in order to fulfill the condition $T \ll \tau_c$ described earlier.

## IV. RESULTS AND DISCUSSION

Figure 3 shows the photon count distributions for the laser light. Four distributions with average count numbers of 1, 4,

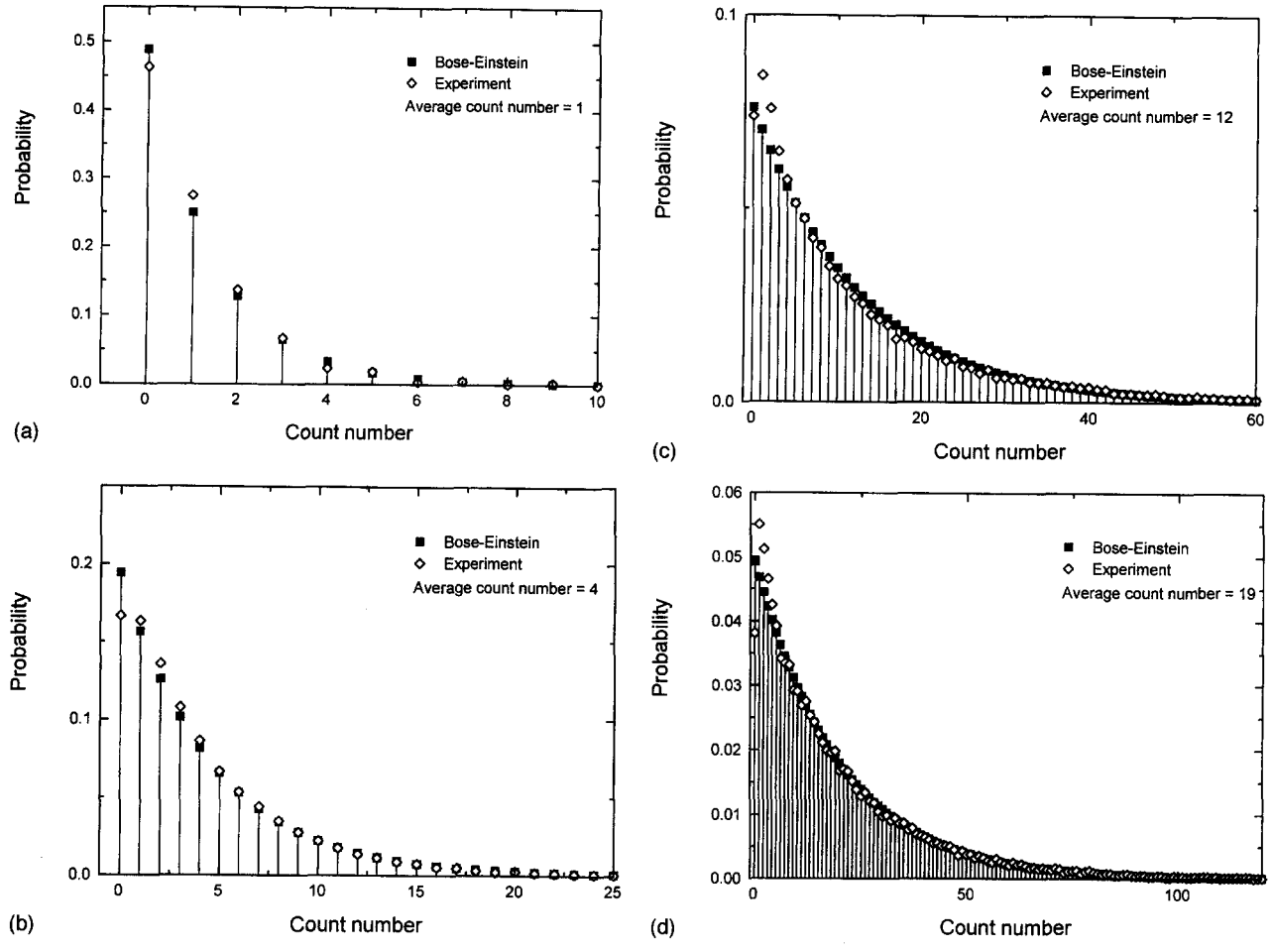


Fig. 4. Experimental photon count distributions (diamonds) for the pseudothermal light and Bose–Einstein distributions (squares) with corresponding average values. (a)–(d) Results for count numbers 1, 4, 12, and 19, respectively.

12, and 19 are shown. Also shown in the picture are Poisson distributions with $\bar{K}$ equal to 1, 4, 12, and 19. As can be seen in the picture, the distributions measured for the He–Ne laser light are almost identical to the Poisson distributions with corresponding average count numbers. This might seem a bit surprising since the laser used in the experiment was not a single longitudinal mode laser and did not emit completely coherent light of constant intensity. Still the photon count distributions are exactly the same as those expected for coherent light. It can be explained as follows. Since the laser operates on a few longitudinal modes simultaneously, the instantaneous intensity varies in time because of mode beating. However the characteristic time of the intensity fluctuations (coherence time $\tau_c$) is relatively short (of the order of 1 ns). Since the shortest time interval $T$ used in the experiment was 1 ms, the relation $T \gg \tau_c$ holds very well, the integrated intensity is constant except for technical noise caused for example by fluctuations of the discharge current in the laser tube, etc., and the experiment yields a Poisson distribution. This shows that one does not need an expensive single-mode He–Ne laser in order to demonstrate the photon count distribution of the coherent light. Such a demonstration can be achieved with a multimode laser at the cost of a somewhat more complex theoretical description. The data in Fig. 3 show the importance of shot noise in the measurements of very low light fluxes. The variance of the photon count number for the Poisson distribution varies as $\sqrt{\bar{K}}$, and thus the signal to noise ratio scales as

$$\mathrm{S/N} = \sqrt{\bar{K}}. \tag{6}$$

Thus the shot noise is the major problem whenever the light intensity and the count number are low. This is where squeezed states with possible sub-Poissonian distributions are most relevant. For very high light intensities and thus high values of $\bar{K}$, one can usually neglect shot noise altogether. This corresponds to the limit in which the coherent state describes the classical monochromatic wave. The results of measurements for pseudothermal light are shown in Fig. 4. The average count numbers shown are again 1, 4, 12, and 19. Also shown in the picture are theoretical distributions (Bose–Einstein distributions) with corresponding average count numbers. The overall agreement is very good although a slight discrepancy can be seen for low count numbers indicating that the light scattered by rotating ground-glass plate used in our experiment is not perfect pseudothermal light. The comparison of Figs. 3 and 4 shows a dramatic difference between the two distributions. The most striking property of the Bose–Einstein distribution, as compared to the Poisson distribution, is that its variance is

larger than the average value and the signal to noise ratio given by the formula

$$S/N = \sqrt{\frac{\bar{K}}{1+\bar{K}}} \tag{7}$$

is always smaller than 1. In this case the noise observed in the photon counting experiment is, for larger values of $\bar{K}$, totally dominated by the fluctuations of the light intensity, while the stochastic nature of the photoelectron process itself manifests itself only for very small values of $\bar{K}$.

In conclusion, we have described a photon counting experiment for the advanced student physics laboratory that demonstrates both shot noise for a constant intensity source and intensity noise for thermal radiation.


[1]D. F. Walls, "Squeezed states of light," Nature **306** (5939), 141–146 (1983).

[2]G. Wentzel, "Über die Richtungsverteilung der Photoelektronen," Z. Phys. **41**(1), 828–832 (1927).

[3]A. Einstein, Ann. Phys. **17**, 132 (1905).

[4]M. O. Scully and M. Sargent III, "The concept of the photon," Phys. Today **25**(3), 38–47 (1972).

[5]H. J. Kimble, M. Dagenais, and L. Mandel, "Photon anti-bunching in resonance fluorescence," Phys. Rev. Lett. **39**(11), 691–695 (1977).

[6]Osamu Hirota (Ed.) *Squeezed Light* (Elsevier, Amsterdam, 1992), pp. 215–220.

[7]L. Mandel, "Fluctuations of photon beams: The distribution of the photoelectrons," Proc. Phys. Soc. **74**(3), 233–243 (1959).

[8]J. W. Goodman, *Statistical Optics* (Wiley, New York, 1985), pp. 238–256, 466–468.

[9]R. Glauber, "Coherent and incoherent states of the radiation field," Phys. Rev. **131**(6), 2766–2788 (1963).

[10]R. Loudon, *The Quantum Theory of Light* (Clarendon, Oxford, 1983), 2nd ed., p. 151.

[11]E. Jakeman, C. J. Oliver, and E. R. Pikem, "A measurement of optical linewidth by photon counting statistics," J. Phys. A (Proc. Phys. Soc.) **1**(3), 406–408 (1968).

[12]W. Martienssen and E. Spiller, "Coherence and fluctuations in light beams," Am. J. Phys. **32**(12), 919–926 (1964).


# Photon states made easy: A computational approach to quantum radiation theory


I. D. Johnston

*School of Physics, University of Sydney, N.S.W. 2006, Australia*



(Received 20 January 1995; accepted 17 October 1995)



Students first meet the wave-particle paradox through the photon and wave descriptions of light. Yet, in basic courses on quantum mechanics, they study matter particles only, because the mathematics of the quantized radiation field is usually considered too advanced. An oscillating electromagnetic field is formally similar to a harmonic oscillator, whose energy eigenstates can represent states of well-defined photon number. Using a computer program from the CUPS project, an approach will be described which demonstrates the action of the annihilation operator on these states, constructs coherent states which behave like classical electromagnetic fields, and shows how such states can be squeezed. All of these have practical relevance in modern optics. This is just one example of the computer making a hitherto unapproachable subject accessible to ordinary undergraduates. Computers have already changed how much of quantum mechanics is taught. As more such possibilities are realized, the teaching of the whole subject must surely change radically. © *1996 American Association of Physics Teachers.*


## I. INTRODUCTION

In the 70 or so years since the original formulation of quantum mechanics, the way the subject is taught has become highly standardized. Almost without exception, all post-introductory textbooks arrange their material in the same way. In particular, they start with one dimensional topics and introduce as many concepts as they can until it becomes too difficult, mathematically, to go further.

In recent years, much software has been written for use in standard courses,[1] to relieve the dependence on extensive analytical expertise which so many students do not have. Nowadays it is easy to generate solutions of problems like bound states in different potential wells, plane waves incident on various barriers, and the motion of wave packets. As a result, instructors able to push the study of one-dimensional quantum mechanics much further than they once could.

Another feature of the standard approach is the prominence given to the idea that the same physical system can be described by different formalisms. The harmonic oscillator, for example, is often treated in three different ways: in Schrödinger representation, in matrix mechanics, and by operator methods. The idea that *different* physical systems can be modeled by the *same mathematics* is equally valuable but seldom exploited. A good example occurs in the quantum theory of radiation.

When most students are introduced to modern physics, the

Michał Karpiński

# BADANIE STATYSTYK ZLICZEŃ FOTONÓW – III PRACOWNIA Z OPTYKI

W ramach ćwiczenia wyznaczyłem statystyki zliczeń fotonów światła laserowego i termicznego oraz wykazałem, że statystyki te pozostają niezmienione po przejściu światła przez płytkę światłodzielącą. Zbadałem też zależność liczby stopni swobody światła termicznego od czasu zliczania fotonów i na tej podstawie wyznaczyłem jego czas koherencji.

## Wstęp

Statystyka zliczeń fotonów światła wytwarzanego przez jednomodowy laser opisana jest rozkładem Poissona [1]:

$$P(N) = \frac{(\bar{N})^N}{N!} \mathrm{e}^{-\bar{N}} \tag{1}$$

gdzie: $P(N)$ – prawdopodobieństwo zliczenia $N$ fotonów; $\bar{N}$ – średnia liczba zliczonych fotonów.

Statystyka zliczeń fotonów światła termicznego opisana jest (w pewnym przybliżeniu, por. [1], rozdz. 6) tzw. rozkładem ujemnym dwumianowym:

$$P(N) = \frac{\Gamma(N+M)}{\Gamma(N+1)\Gamma(M)} \left(1+\frac{M}{\bar{N}}\right)^{-N} \left(1+\frac{\bar{N}}{M}\right)^{-M} \tag{2}$$

gdzie: $\Gamma(x)$ – funkcja gamma Eulera; $M$ – parametr rozkładu, tzw. liczba stopni swobody.

Liczba stopni $M$ swobody w granicy długich czasów zliczania jest równa stosunkowi czasu zliczania do czasu koherencji światła termicznego. W przypadku światła niespójnego przestrzennie $M$ jest dodatkowo pomnożone przez ilość przestrzennych stopni swobody (por. [1], rozdz. 9). W przypadku czasów zliczania krótszych od czasu koherencji (i pełnej spójności przestrzennej) $M$ dąży do jedności, a rozkład ujemny dwumianowy redukuje się do rozkładu Bosego-Einsteina (p. załącznik):

$$P(N) = \frac{1}{1+\bar{N}} \left(\frac{\bar{N}}{1+\bar{N}}\right)^N \tag{3}$$

Rozważmy teraz, jak zmieni się statystyka zliczeń fotonów po przejściu światła przez płytkę światłodzielącą o współczynniku transmisji $T$. Zgodnie z obliczeniami przedstawionymi w załączniku, statystyka światła laserowego pozostanie poissonowska, a statystyka światła termicznego nadal będzie statystyką opisaną rozkładem ujemnym dwumianowym o niezmienionej liczbie stopni swobody $M$ (wynika z tego, że również statystyka Bosego-Einsteina pozostanie statystyką Bosego-Einsteina). Zmieni się jedynie średnia liczba zliczeń: z $\bar{N}$ na $T\bar{N}$.

## Układ doświadczalny

Układ eksperymentalny do pomiarów ze światłem laserowym przedstawiony jest na rys. 1a. Źródłem światła był laser He-Ne, emitujący światło o długości fali 632,8 nm. Laser nie był jednomodowy, ale ponieważ czasy zliczania były dłuższe niż charakterystyczne czasy dudnień spowodowanych przez interferencję różnych modów, uzyskiwane statystyki były poissonowskie. Wiązka laserowa była odbijana od zwierciadła płaskiego M1 i przepuszczana przez serię filtrów szarych (NF), zmniejszających natężenie wiązki do poziomu nieszkodliwego dla detektora ( $< 10^6$ fotonów/s). Dalsza część układu była umieszczona w możliwie szczelnej

osłonie z czarnego PCW. Wiązka przechodziła dalej przez filtr interferencyjny IF ($\lambda$ = 631 nm, $\Delta\lambda$ = 9 nm), była odbijana od zwierciadła M2 i ogniskowana przez soczewkę skupiającą LE o ogniskowej 15 cm. Następnie na drodze wiązki znajdowała się (usuwalna) płytka światłodzieląca (BS). Część wiązki odbita od płytki była pochłaniana przez pochłaniacz wiązki (S); druga część przez polaryzator P kierowana była do detektora D, umieszczonego w ognisku soczewki LE. Detektorem był licznik pojedynczych fotonów (SPCM AQ 131, EG&G Canada). Charakterystyka detektora: ciemne zliczenia max. 250 fotonów/s, czas martwy max. 50 ns. Detektor był chłodzony wodą. Sygnały z detektora poprzez wzmacniacz i wydłużacz impulsów kierowane były do licznika karty National Instruments PCI 6040 E. Długość czasu zliczania była regulowana przy pomocy wewnętrznego zegara karty; minimalny dostępny czas zliczania wynosił 1 μs.

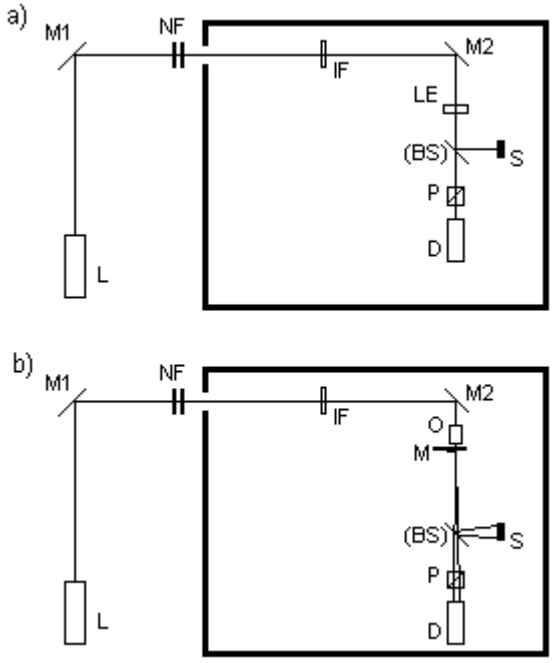


**Rys. 1** Schemat układu doświadczalnego do pomiarów dla: a) światła laserowego; b) światła termicznego. L – laser; M1, M2 – zwierciadła płaskie; NF – filtry szare; IF – filtr interferencyjny; LE – soczewka; O – obiektyw; M – obracająca się matówka; BS – płytka światłodzieląca; S – pochłaniacz wiązki; P – polaryzator; D – detektor.

Do pomiarów statystyk światła termicznego konieczna była niewielka modyfikacja układu, przedstawiona na rys. 1b. Ponieważ naturalne światło termiczne ma bardzo krótki czas koherencji (poniżej pikosekund) dysponując minimalnym czasem zliczania 1 μs rejestrowałbym rozkład ujemny dwumianowy o liczbie stopni swobody $M$ rzędu $10^6$ lub więcej – dla tak dużych wartości $M$ rozkład ujemny dwumianowy staje się w praktyce rozkładem Gaussa. Aby uzyskać rozkład możliwie bliski rozkładowi Bosego-Einsteina potrzebne było światło termiczne o czasie koherencji dłuższym niż 1 μs. Światło takie otrzymuje się ogniskując wiązkę lasera na poruszającej się powoli matówce ([1], par. 4.4.3). W miejscu soczewki umieszczony został obiektyw mikroskopu O (powiększenie 12 razy) – w celu lepszego zogniskowania wiązki. Za obiektywem, w ognisku, znajdowała się okrągła matówka M, obracana powoli przez silnik elektryczny. Pozostałe elementy układu pozostały niezmienione, jedynie detektor został maksymalnie odsunięty od matówki, by zbierać światło możliwie spójne przestrzennie. Detektor został również przesunięty nieco w bok w stosunku do wiązki laserowej.

Przed przystąpieniem do właściwych pomiarów należało upewnić się, czy średnica wiązki w ognisku soczewki jest mniejsza niż średnica powierzchni detektora (dla pomiarów ze światłem laserowym). W tym celu w ognisku soczewki przeprowadziłem pomiar średnicy wiązki przy pomocy ostrza brzytwy. Otrzymałem wynik ok. 100 μm. Średnica powierzchni światłoczułej detektora wynosi 170 μm, a więc wiązka była dostatecznie dobrze zogniskowana.

**Wyniki pomiarów i wnioski**

Jako pierwsze wyznaczyłem statystyki dla światła laserowego dla różnych czasów zliczania $t$ oraz różnych średnich liczb zliczeń $\bar{N}$. Podczas tej części eksperymentu płytka

światłodzieląca była usunięta z drogi wiązki. Wyniki w postaci histogramów wraz z dopasowanymi rozkładami Poissona przedstawione są na rys. 2. Czasy zliczania były na tyle krótkie, że zliczenia ciemne (na poziomie 250 Hz) były do pominięcia. Za każdym razem wykonane zostało 100 000 powtórzeń.

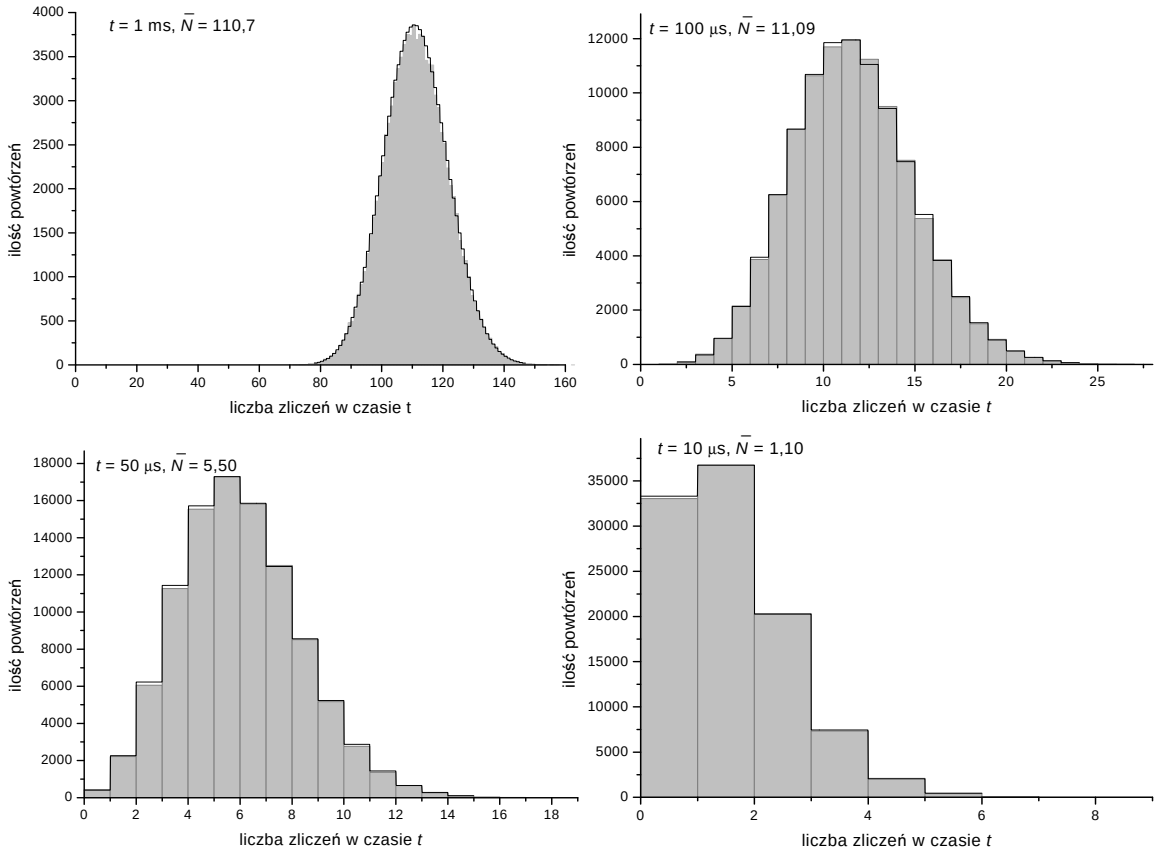


**Rys. 2** Histogramy liczby zliczeń fotonów światła laserowego dla czasów zliczania w zakresie 10 μs – 1 ms.

Dopasowania rozkładu Poissona do danych doświadczalnych jest bardzo dobre: dla każdego z 4 czasów zliczania współczynnik korelacji $R^2$ był większy niż 0,999. Niewielkie rozbieżności mogą być spowodowane: a) dryfem natężenia lasera w czasie; b) faktem, że laser nie jest jednomodowy; c) skończoną ilością powtórzeń.

Następnie pomiędzy soczewką a detektorem umieściłem płytkę światłodzielącą i zmierzyłem odpowiednie statystyki (z tymi samymi czasami zliczania i taką samą liczbą powtórzeń), przedstawione na rys. 3. Zgodnie z przewidywaniami teoretycznymi otrzymujemy również rozkład Poissona. Dopasowanie rozkładu Poissona do danych doświadczalnych jest bardzo dobre: za każdym razem współczynnik $R^2 > 0{,}9999$.

W tabeli 1 zamieszczone są średnie liczby zliczeń z pomiarów bez oraz z płytką światłodzielącą (odpowiednio $N_1$ oraz $N_2$), a także obliczona na tej podstawie wartość współczynnika transmisji płytki $T = N_2/N_1$.

| czas zliczania $t$ (μs) | $N_1$ | $N_2$ | $T$ |
|---|---|---|---|
| 1000 | 110,712 | 24,316 | 0,220 |
| 100 | 11,093 | 2,463 | 0,222 |
| 50 | 5,500 | 1,219 | 0,222 |
| 10 | 1,103 | 0,251 | 0,228 |

**Tabela 1** $N_i$ **–** średnia liczba zliczeń: 1 – bez, 2 – z płytką światłodzielącą; $T$ **–** transmisja płytki.

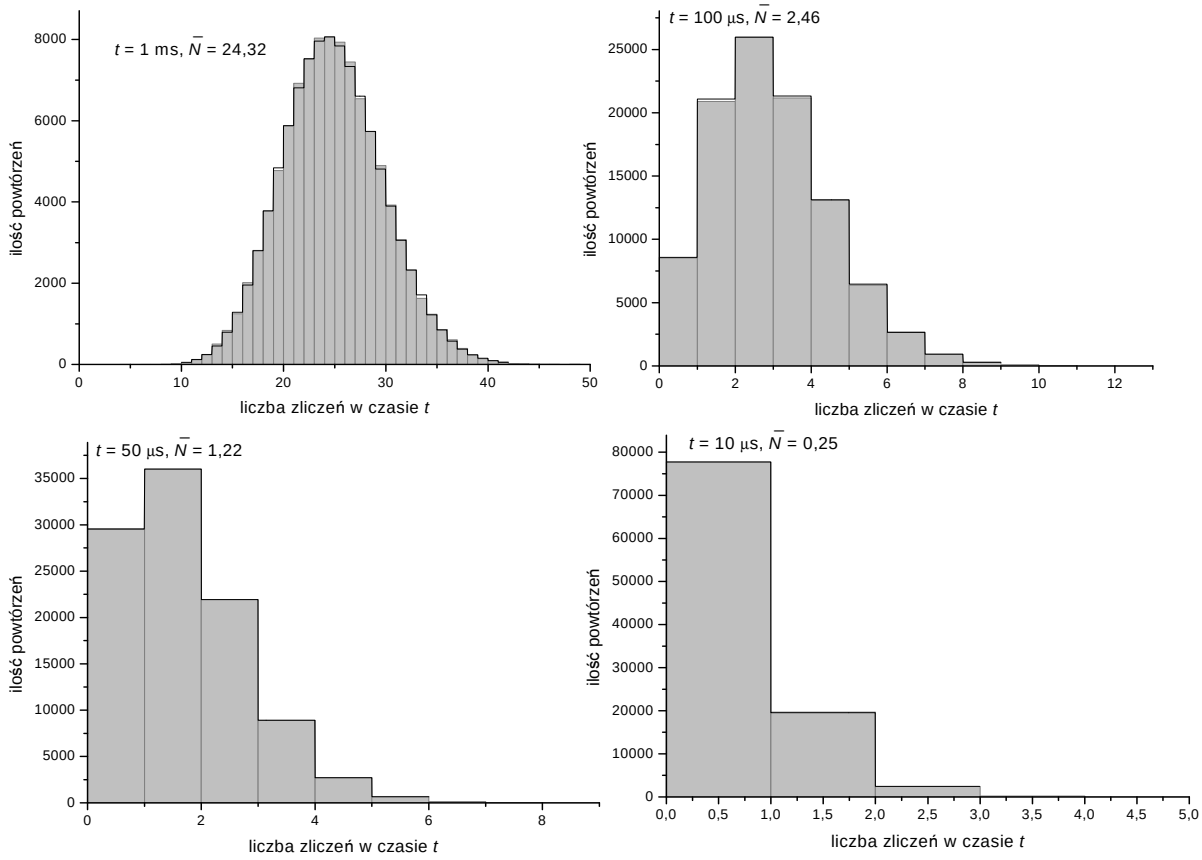


**Rys. 3** Histogramy dla światła laserowego po przejściu przez płytkę światłodzielącą.

Otrzymujemy średnią wartość $T = 0{,}223 \pm 0{,}004$. Rozbieżności pomiędzy otrzymanymi wartościami $T$ pojawiają się na 3. miejscu znaczącym, różnica pomiędzy wartością maksymalną i minimalną wynosi 3,6%. Najprawdopodobniej przyczyną rozbieżności są niestabilności pracy lasera – natężenia lasera zmieniało się w niewielkim stopniu z upływem czasu.

Drugą częścią ćwiczenia było wyznaczenie statystyk zliczeń fotonów dla światła termicznego. Starałem się uzyskać statystykę zliczeń opisaną rozkładem Bosego-Einsteina – do tego celu potrzebne było światło termiczne o możliwie długim czasie koherencji. Obracając matówkę (por. zmodyfikowany układ doświadczalny, rys. 1b) z bardzo niewielką prędkością udawało się uzyskać czas koherencji nie mniejszy niż 6 ms (sposób pomiaru czasu koherencji omówiony zostanie w następnym akapicie). Można by się w takim razie spodziewać, że dla czasów zliczania rzędu mikrosekund statystyka zliczeń fotonów będzie opisywana rozkładem Bosego-Einsteina. Niestety okazało się, że uzyskiwane światło termiczne nawet dla krótkiego czasu zliczania jest w pewnym stopniu niespójne czasowo lub przestrzennie (minimalna możliwa do osiągnięcia ilość stopni swobody $M$ wynosiła ok. 3). Zredukowanie tej niespójności (dalsze odsunięcie detektora od matówki i silniejsze zogniskowanie wiązki na matówce) było trudne technicznie. Z tego powodu zmierzone statystyki są opisywane rozkładem ujemnym dwumianowym. Jednakże, ponieważ rozkład Bosego-Einsteina jest szczególnym przypadkiem rozkładu ujemnego dwumianowego, wykazanie, że rozkład ten w przypadku ogólnym (dla różnych $M$) nie zmienia się po przejściu światła przez płytkę, implikuje, że szczególny przypadek tego rozkładu – rozkład Bosego-Einsteina – po przejściu przez płytkę też pozostanie niezmieniony.

Przed przystąpieniem do właściwych pomiarów zmierzyłem czas koherencji uzyskiwanego przeze mnie światła termicznego. W tej części eksperymentu płytka światłodzieląca była usunięta z drogi światła. Zmierzyłem statystyki zliczeń fotonów dla szerokiego zakresu czasów zliczania. Na podstawie uzyskanych histogramów obliczałem rozkłady prawdopodobieństwa i dopasowywałem do nich rozkład ujemny dwumianowy (2). Na wykresie (rys. 4) przedstawiona jest zależność liczby stopni swobody $M$ od czasu zliczania $t$. Jak widać, w szerokim zakresie czasów (1 μs – 10 ms) $M$ nie zależy od czasu zliczania, wykazuje jedynie przypadkowe fluktuacje w zakresie 2,8 – 4,8. Zależność $t(M)$ pojawia się dopiero dla czasów $t$ dłuższych od 10 ms. Zależność ta jest liniowa, co przedstawione zostało, wraz z dopasowaną prostą, na rys. 5. Na podstawie równania prostej można wyznaczyć czas koherencji światła. Zgodnie z [1], rozdz. 6 i 9, dla czasów zliczania dużo dłuższych od czasu koherencji $\tau_c$ zachodzi związek: $M = \frac{t}{\tau_c}$. W przypadku braku spójności przestrzennej zależność ta modyfikuje się do $M = M_s \frac{1}{\tau_c} t$, gdzie $M_s$ jest liczbą przestrzennych stopni swobody. Okazuje się jednak, że zmierzona przeze mnie zależność $M(t)$ ma inną postać: jest liniowa, ale nie wprost proporcjonalna:

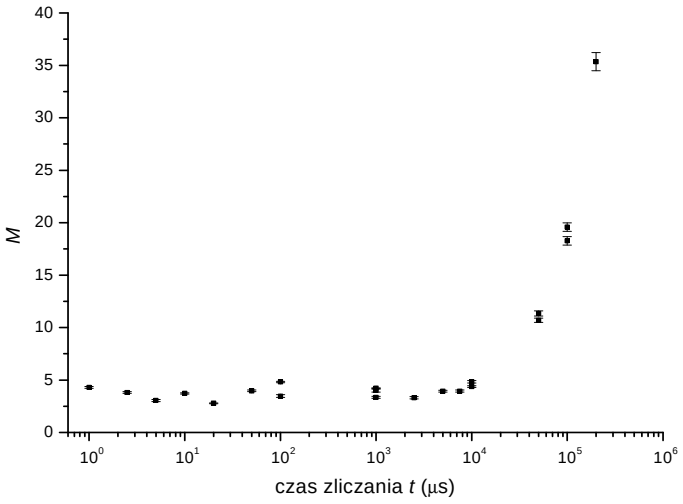


**Rys. 4** Wykres zależności liczby stopni swobody $M$ od czasu zliczania $t$.

$$M = M_s \frac{1}{\tau_c} + M_0 \qquad (4)$$

Zakładając pełną koherencję przestrzenną ($M_s$ = 1) można obliczyć ograniczenie dolne na czas koherencji, jako odwrotność współczynnika kierunkowego dopasowanej prostej: $\tau_c = 6{,}23 \pm 0{,}09$ ms. Jeśli w rzeczywistości światło jest niespójne przestrzennie ($M_s > 1$), czas koherencji jest dłuższy. W przypadku tego eksperymentu istotny jest fakt, że dostępne są czasy zliczania krótsze od czasu koherencji, więc wystarczająca jest znajomość ograniczenia dolnego na $\tau_c$.

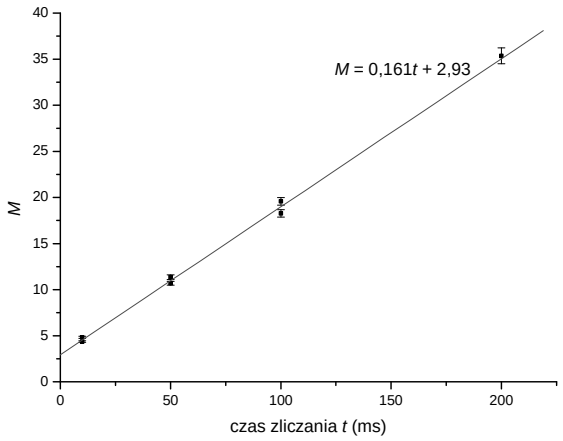


**Rys. 5** Wykres zależności $M(t)$ dla wolno obracającej się matówki.

Komentarza wymaga jeszcze obecność w zależności $M(t)$ członu $M_0$. O ten niezależny od czasu zliczania człon powiększone są wartości $M$ dla wszystkich pomiarów. Członu takiego nie przewidują obliczenia w [1]. Niezależność tego członu od czasu sugeruje, że pochodzi on od promieniowania o bardzo długim czasie koherencji – a więc od promieniowania laserowego. Wydaje się prawdopodobne, że to właśnie wartość tego członu fluktuuje w czasie – tłumaczy to rozrzut wartości $M$ dla 1 μs < $t$ < 10 ms oraz różnice wartości $M$ (rzędu ±1,06, jako błąd przyjmuję dwa odchylenia standardowe wartości $M$ dla

1 μs < $t$ < 10 ms) w przypadku powtórzeń pomiarów dla czasów $t$ > 10 ms. Tak silne fluktuacje wskazują, że ich źródłem może być obracająca się matówka, która nie jest zupełnie jednorodna. Podejrzewam więc, że człon $M_0$ pojawia się w wyniku przedostawania się przez matówkę pewnej ilości „nieutermicznionego" światła laserowego. W praktyce obecność tego członu powoduje, że, nawet dla czasów zliczania znacznie krótszych od $\tau_c$, $M > 1$.

Aby sprawdzić poprawność wyznaczania czasu koherencji wykonałem analogiczną serię pomiarów dla szybciej obracającej się matówki. Oczekiwałem zmniejszenia się czasu koherencji. Wyniki pomiarów przedstawione są na rys. 6. Zależność $M(t)$ jest liniowa dla czasów $t > 1$ ms. Czas koherencji wynosi $\tau_c = 1{,}24 \pm 0{,}03$ i zgodnie z oczekiwaniami jest krótszy od czasu dla wolno obracającej się matówki.

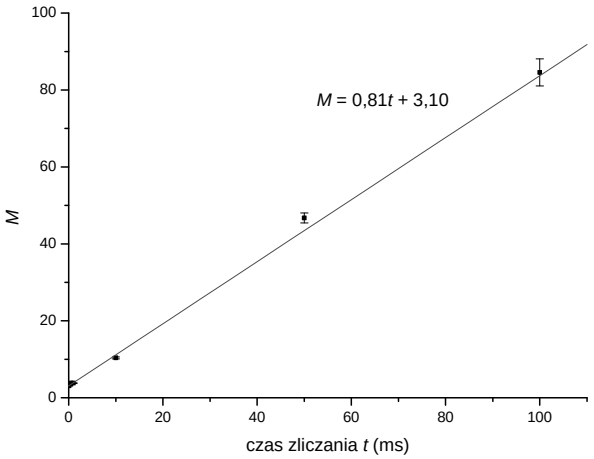


**Rys. 6** Wykres zależności $M(t)$ dla szybko obracającej sie matówki.

Znając parametry dostępnego światła termicznego mogłem przystąpić do właściwej części pomiarów. Wykonałem pomiary statystyk zliczeń fotonów dla 4 różnych czasów zliczania. Odpowiednie histogramy zamieszczone są na rys. 7. Obok histogramów znajdują się wyliczone na ich podstawie rozkłady prawdopodobieństwa i dopasowane do nich krzywe odpowiadające rozkładowi ujemnemu dwumianowemu (2).

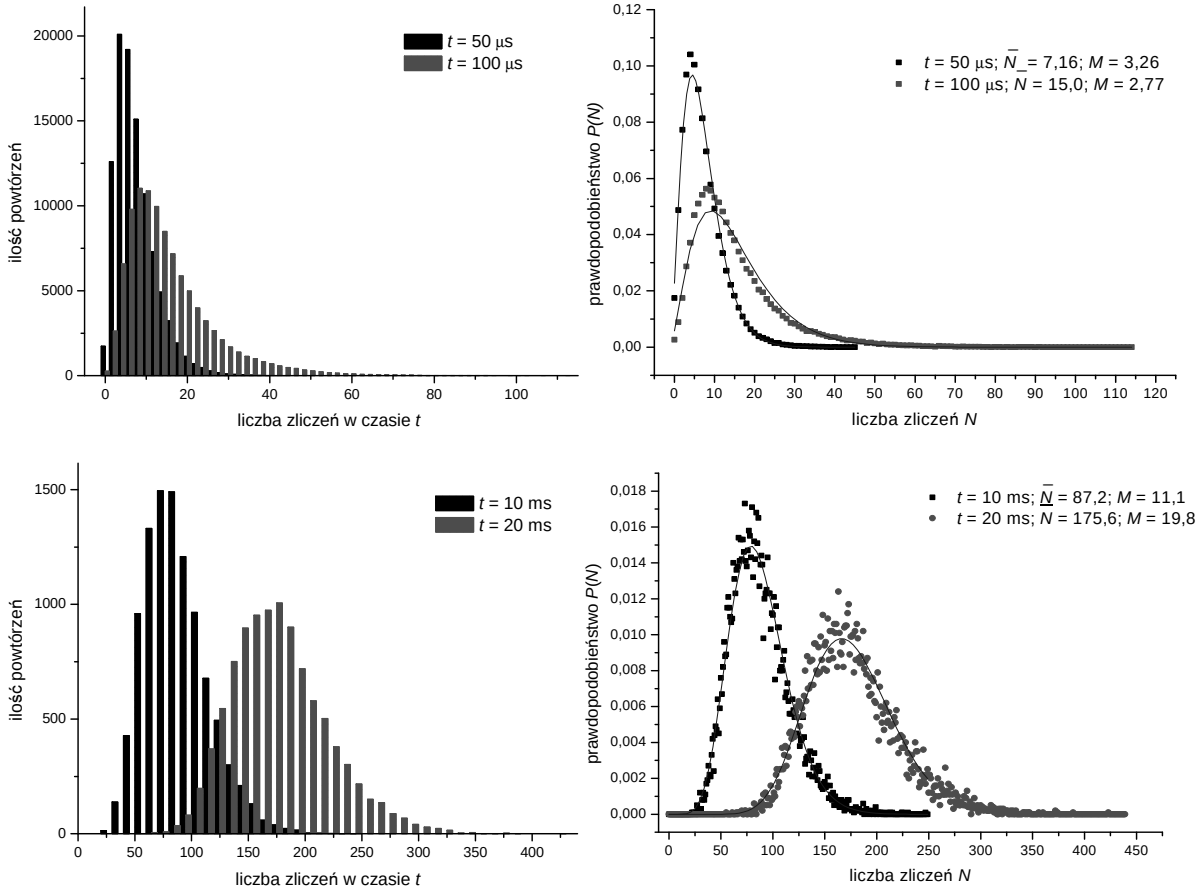


**Rys. 7** Histogramy zliczeń fotonów dla światła termicznego i dopasowane krzywe (rozkład ujemny dwumianowy).

Dopasowanie jest dobre ($R^2 > 0{,}975$), ale nie tak dobre jak dla światła laserowego. Przyczyną tego (oprócz wymienianych już wcześniej powodów) są następujące fakty: a) rozkład ujemny dwumianowy tylko w przybliżeniu opisuje statystykę światła termicznego ([1], rozdz. 6); b) ze względu na czas trwania pomiarów dla $t$ = 10 ms i 20 ms wykonano tylko 10000 powtórzeń; c) dla pomiarów z $t$ = 10 ms i 20 ms konieczne było odejmowanie od wyników uśrednionej wartości tła (ciemnych zliczeń).

Następnie na drodze światła do detektora umieściłem płytkę światłodzielącą i nie zmieniając natężenia światła wykonałem pomiary statystyk zliczeń dla tych samych czasów zliczania. Wyniki przedstawiłem na rys. 8.

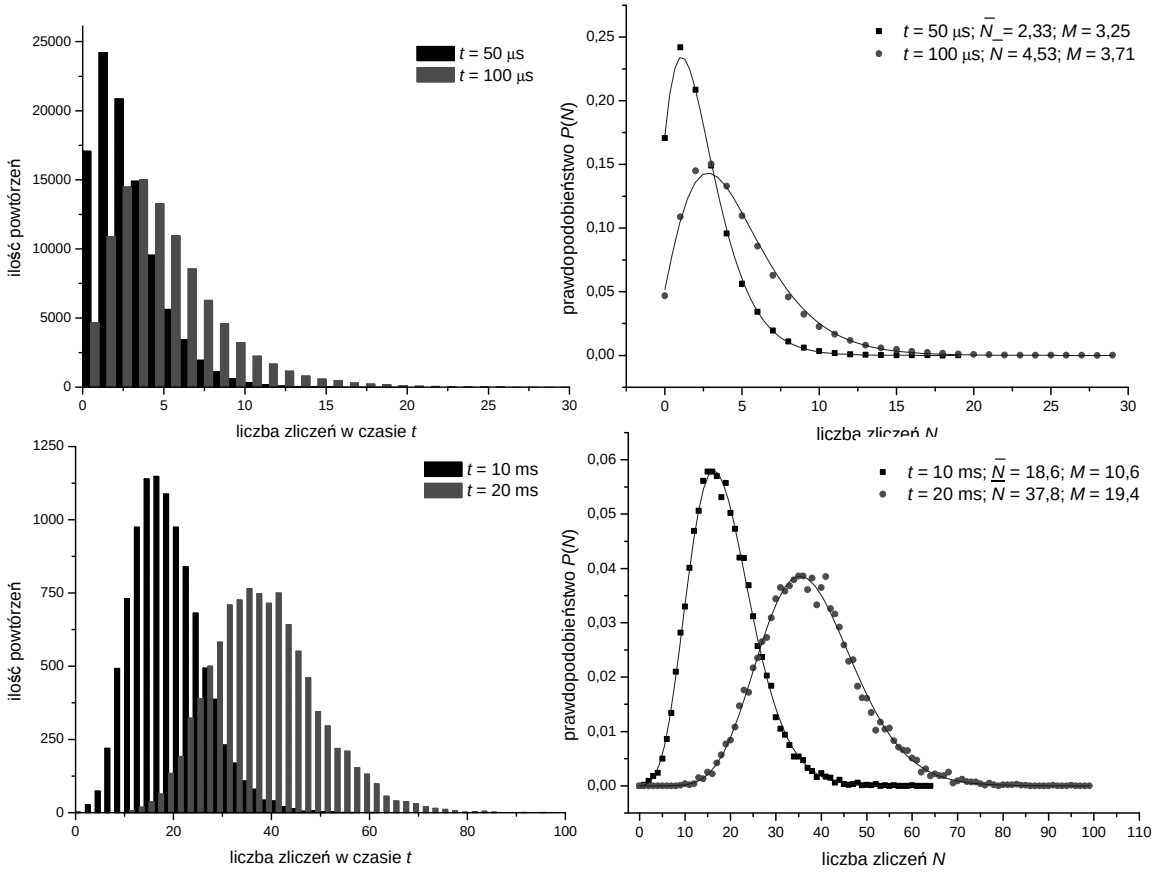


**Rys. 8** Histogramy dla światła termicznego po przejściu przez płytkę światłodzielącą i dopasowane krzywe (rozkład ujemny dwumianowy).

| $t$ | $M_1$ | $M_2$ |
|---|---|---|
| 50 μs | 3,26 | 3,25 |
| 100 μs | 2,77 | 3,71 |
| 10 ms | 11,1 | 10,6 |
| 20 ms | 19,8 | 19,4 |

**Tabela 2** $t$ – czas zliczania; $M_i$ – liczba stopni swobody: 1 – bez, 2 – z płytką światłodzielącą

Również po przejściu światła przez płytkę światłodzielącą obserwujemy statystyki opisywane rozkładem ujemnym dwumianowym. W tabeli 2 zamieszczone zostało porównanie parametrów $M$ odpowiednich par rozkładów.

Wartości $M$ dla pomiarów z i bez płytki światłodzielącej są sobie bliskie, chociaż w większości przypadków różne (w granicach ±1). Różnice te są najprawdopodobniej spowodowane omawianymi wcześniej fluktuacjami $M$ (których rozrzut wynosi ±1,06).

**Podsumowanie**

W wyniku pomiarów potwierdzone zostały przewidywania teoretyczne – zarówno statystyka zliczeń fotonów światła lasera jednomodowego, jak i światła termicznego pozostaje nie zmieniona (za wyjątkiem wartości średniej) po przejściu światła przez płytkę światłodzielącą. W przypadku światła termicznego pokazane zostało, że, w granicach błędu doświadczalnego, nie zmieniona pozostaje również liczba stopni swobody $M$. Wyznaczona została także zależność liczby stopni swobody $M$ światła termicznego od czasu zliczania $t$ i na jej podstawie obliczony czas koherencji $\tau_c$ (dokładniej: ograniczenie dolne na czas koherencji). Zależność $M(t)$, zgodnie z przewidywaniami [1], jest liniowa. Nie jest jednak wprost proporcjonalna – pojawia się fluktuujący w czasie składnik (o niezależnej od $t$ wartości średniej), powodujący fluktuacje wartości $M$. Podejrzewam, jak już uzasadniałem wcześniej, że jego obecność jest spowodowana przez niepełne rozpraszanie światła laserowego na matówce.

**Literatura:**

[1] J. W. Goodman, *Optyka statystyczna*, PWN, Warszawa 1993;
[2] W. Vogel et al., *Quantum optics: an introduction*, Wiley-VCH, Berlin 2001;
[3] R. J. Nowak, *Statystyka matematyczna*, Wydział Fizyki UW 1999.

ZAŁĄCZNIK

1) Światło lasera jednomodowego

Światło lasera jednomodowego kwantowomechanicznie opisywane jest przez tzw. stan koherentny, będący kombinacją liniową stanów jednofotonowych ze współczynnikami równymi odpowiednim prawdopodobieństwom z rozkładu Poissona [2]:

$$|\bar{N}> = \sum_{N=0}^{\infty} \frac{\bar{N}^N}{N!} e^{-\bar{N}} |N> \tag{A.1}$$

gdzie: $|\bar{N}>$ – stan koherentny o średniej liczbie fotonów $\bar{N}$ ; $|N>$ – stan $N$-fotonowy.

Bez problemu jesteśmy w stanie opisać działanie płytki światłodzielącej o współczynniku transmisji $T$ na stan $N$-fotonowy: prawdopodobieństwo przejścia przez płytkę $K$ fotonów jest dane rozkładem dwumianowym. A więc stan |N> po przejściu przez płytkę zmieni się w stan:

$$|N'> = \sum_{K=0}^{N} \binom{N}{K} T^K (1-T)^{N-K} |K> \tag{A.2}$$

Znając działanie płytki na stan jednofotonowy oraz rozkład stanu koherentnego na stany jednofotonowe możemy wypisać postać stanu koherentnego po przejściu przez płytkę:

$$|\bar{N}'> = \sum_{N=0}^{\infty} \sum_{K=0}^{N} \frac{\bar{N}^N}{N!} e^{-\bar{N}} \binom{N}{K} T^K (1-T)^{N-K} |K> \tag{A.3}$$

Aby wyznaczyć statystykę tego stanu, należy wyrazić go jako liniową kombinację stanów jednofotonowych:

$$|\bar{N}'> = \sum_{K=0}^{\infty} a_K |K> \tag{A.4}$$

W celu wyznaczenia postaci współczynników kombinacji liniowej należy zamienić w (A.3) kolejność sumowania. Otrzymujemy wtedy:

$$\begin{aligned} a_K &= \sum_{N=K}^{\infty} \frac{\bar{N}^N}{N!} e^{-\bar{N}} \binom{N}{K} T^K (1-T)^{N-K} = \\ &= \frac{e^{-\bar{N}}}{K!} T^K \sum_{N=K}^{\infty} \frac{\bar{N}^N \cancel{N!}}{\cancel{N!}(N-K)!} (1-T)^{N-K} \end{aligned} \tag{A.5}$$

Dokonujemy przeindeksowania $N \to N + K$:

$$\begin{aligned} a_K &= \frac{e^{-\bar{N}}}{K!} T^K \sum_{N=0}^{\infty} \frac{\bar{N}^{N+K}}{N!} (1-T)^N = \frac{e^{-\bar{N}}}{K!} (T\bar{N})^K \sum_{N=0}^{\infty} \frac{[\bar{N}(1-T)]^N}{N!} = \\ &= \frac{e^{-\bar{N}}}{K!} (T\bar{N})^K \cdot e^{\bar{N}(1-T)} = \frac{e^{-T\bar{N}}}{K!} (T\bar{N})^K \end{aligned} \tag{A.6}$$

(Skorzystaliśmy z rozwinięcia funkcji $e^x$ w szereg Taylora.)

A więc stan światła po przejściu przez płytkę światłodzielącą możemy zapisać jako:

$$|\bar{N}'> = \sum_{K=0}^{\infty} \frac{(T\bar{N})^K}{K!} e^{-T\bar{N}} |K> \tag{A.7}$$

Porównując to wyrażenie z (A.1) zauważamy, że jest to również stan o statystyce poissonowskiej o wartości średniej pomnożonej przez współczynnik transmisji płytki.

2) Światło termiczne

Analogicznie jak dla światła laserowego, stan światła termicznego (o $M$ stopniach swobody) można zapisać jako kombinację liniową stanów jednofotonowych; tym razem

współczynnikami kombinacji będą prawdopodobieństwa z rozkładu ujemnego dwumianowego (2):

$$|\bar{N}> = \sum_{N=0}^{\infty} \frac{\Gamma(N+M)}{\Gamma(N+1)\Gamma(M)} \left(1+\frac{M}{\bar{N}}\right)^{-N} \left(1+\frac{\bar{N}}{M}\right)^{-M} |N> \qquad (A.8)$$

Podobnie jak dla światła laserowego, stan światła termicznego po przejściu przez płytkę światłodzielącą o transmisji $T$ możemy zapisać jako:

$$|\bar{N}'> = \sum_{N=0}^{\infty} \sum_{K=0}^{N} \frac{\Gamma(N+M)}{\Gamma(N+1)\Gamma(M)} \left(1+\frac{M}{\bar{N}}\right)^{-N} \left(1+\frac{\bar{N}}{M}\right)^{-M} \binom{N}{K} T^K (1-T)^{N-K} |K> \qquad (A.9)$$

Podobnie jak poprzednio, aby doprowadzić to wyrażenie do postaci kombinacji liniowej stanów jednofotonowych: $|\bar{N}'> = \sum_{K=0}^{\infty} a_K |K>$ zamieniamy kolejność sumowania i otrzymujemy wyrażenie na $a_K$:

$$a_K = \sum_{N=K}^{\infty} \frac{\Gamma(N+M)}{\Gamma(N+1)\Gamma(M)} \left(1+\frac{M}{\bar{N}}\right)^{-N} \left(1+\frac{\bar{N}}{M}\right)^{-M} \binom{N}{K} T^K (1-T)^{N-K} \qquad (A.10)$$

Aby ułatwić późniejsze przekształcenia warto skorzystać z równości (por. [1], rozdz. 9):

$$\frac{\Gamma(N+M)}{\Gamma(N+1)\Gamma(M)} \left(1+\frac{M}{\bar{N}}\right)^{-N} \left(1+\frac{\bar{N}}{M}\right)^{-M} = \int_0^{\infty} \frac{(\alpha W)^N}{N!\Gamma(M)} \mathrm{e}^{-\alpha W} \left(\frac{M}{\bar{W}}\right)^M W^{M-1} \mathrm{e}^{-M\frac{W}{\bar{W}}} dW \qquad (A.11)$$

gdzie: $\alpha\bar{W} = \bar{N}$; $\alpha$ – parametr. Po podstawieniu do (A.10) i zamianie kolejności sumowania i całkowania otrzymujemy:

$$\begin{aligned}
a_K &= \int_0^{\infty} \sum_{N=K}^{\infty} \frac{(\alpha W)^N}{N!\Gamma(M)} \mathrm{e}^{-\alpha W} \left(\frac{M}{\bar{W}}\right)^M W^{M-1} \mathrm{e}^{-M\frac{W}{\bar{W}}} \frac{N!}{(N-K)!K!} T^K (1-T)^{N-K} dW = \\
&= \int_0^{\infty} \frac{\mathrm{e}^{-\alpha W}}{\Gamma(M)K!} \left(\frac{M}{\bar{W}}\right)^M W^{M-1} \mathrm{e}^{-M\frac{W}{\bar{W}}} T^K (\alpha W)^K \sum_{N=K}^{\infty} \frac{(\alpha W)^{N-K}(1-T)^{N-K}}{(N-K)!} dW = \\
&= \int_0^{\infty} \frac{\mathrm{e}^{-\alpha W}}{\Gamma(M)K!} \left(\frac{M}{\bar{W}}\right)^M W^{M-1} \mathrm{e}^{-M\frac{W}{\bar{W}}} (T\alpha W)^K \sum_{N=0}^{\infty} \frac{[\alpha W(1-T)]^N}{N!} dW = \\
&= \int_0^{\infty} \frac{\mathrm{e}^{-\alpha W}}{\Gamma(M)K!} \left(\frac{M}{\bar{W}}\right)^M W^{M-1} \mathrm{e}^{-M\frac{W}{\bar{W}}} (T\alpha W)^K \mathrm{e}^{\alpha W(1-T)} dW = \\
&= \int_0^{\infty} \frac{(T\alpha W)^K}{\Gamma(M)K!} \mathrm{e}^{-T\alpha W} \left(\frac{M}{\bar{W}}\right)^M W^{M-1} \mathrm{e}^{-M\frac{W}{\bar{W}}} dW = \left| \begin{array}{l} \text{zamiana zmiennych:} \\ W' = TW \\ dW = \frac{dW'}{T} \end{array} \right| = \\
&= \int_0^{\infty} \frac{(\alpha W')^K}{\Gamma(M)K!} \mathrm{e}^{-\alpha W'} \left(\frac{M}{\bar{W}}\right)^M \frac{W'^{M-1}}{T^{M-1}} \mathrm{e}^{-M\frac{W'}{T\bar{W}}} \frac{1}{T} dW' = \\
&= \int_0^{\infty} \frac{(\alpha W')^K}{K!\Gamma(M)} \mathrm{e}^{-\alpha W'} \left(\frac{M}{T\bar{W}}\right)^M W'^{M-1} \mathrm{e}^{-M\frac{W'}{T\bar{W}}} dW'
\end{aligned} \qquad (A.12)$$

Korzystając znów z (A.11) otrzymujemy:

$$a_K = \frac{\Gamma(K+M)}{\Gamma(K+1)\Gamma(M)} \left(1+\frac{M}{T\bar{N}}\right)^{-K} \left(1+\frac{T\bar{N}}{M}\right)^{-M} \qquad (A.13)$$

A więc statystyka promieniowania termicznego po przejściu przez płytkę światłodzielącą jest nadal określona rozkładem ujemnym dwumianowym o niezmienionej liczbie stopni swobody $M$ i średniej liczbie fotonów równej $T\bar{N}$ :

$$|\bar{N}> = \sum_{K=0}^{\infty} \frac{\Gamma(K+M)}{\Gamma(K+1)\Gamma(M)} \left(1+\frac{M}{T\bar{N}}\right)^{-K} \left(1+\frac{T\bar{N}}{M}\right)^{-M} |K> \qquad \text{(A.14)}$$

3) Redukcja rozkładu ujemnego dwumianowego do rozkładu Bosego-Einsteina

Rozkład prawdopodobieństwa dla rozkładu ujemnego dwumianowego dany jest przez:

$$P(N) = \frac{\Gamma(N+M)}{\Gamma(N+1)\Gamma(M)} \left(1+\frac{M}{\bar{N}}\right)^{-N} \left(1+\frac{\bar{N}}{M}\right)^{-M} \qquad \text{(A.15)}$$

Dla $M \to 1$:

$$P(N) \to \left(1+\frac{1}{\bar{N}}\right)^{-N} \frac{1}{1+\bar{N}} = \frac{1}{1+\bar{N}} \left(\frac{\bar{N}}{\bar{N}+1}\right)^{N} \qquad \text{(A.16)}$$

otrzymujemy rozkład Bosego-Einsteina (3).

ZAŁĄCZNIK B

Spróbujmy teraz zbadać, w ogólnym przypadku, jaka powinna być statystyka natężenia światła, by płytka światłodzieląca nie powodowała jej zmiany.

Załóżmy, że rozkład prawdopodobieństwa dla natężenia całkowego $W$ dany jest funkcją $\rho(W;\bar{W})$ (dla $W \geq 0$, dla W < 0 prawdopodobieństwo jest oczywiście zerowe), gdzie parametr $\bar{W}$ jest średnią wartością natężenia całkowego:

$$\bar{W} = \int_0^\infty W \rho(W;\bar{W}) dW \tag{B.1}$$

(Wartość $\bar{W}$ jest wprost proporcjonalna do średniej liczby fotonów $\bar{N}$ : $\bar{N} = \alpha\bar{W}$ )

Znając $\rho(W;\bar{W})$ możemy (zgodnie z [1], rozdz. 9) zapisać współczynniki rozwinięcia stanu światła na stany jednofotonowe:

$$|\bar{N}> = \sum_{N=0}^{\infty} a_N |N>; \quad a_N = \int_0^\infty \frac{(\alpha W)^N}{N!} \mathrm{e}^{-\alpha W} \rho(W;\bar{W}) dW \tag{B.2}$$

Podobnie jak poprzednio, zapiszmy działanie płytki światłodzielącej o transmisji $T$ na jednofotonowy stan światła $|N>$ [por. równ. (A.2)]:

$$|N'> = \sum_{K=0}^{N} \binom{N}{K} T^K (1-T)^{N-K} |K> \tag{B.3}$$

gdzie |N'> oznacza stan jednofotonowy po przejściu przez płytkę. A zatem płytka światłodzieląca przekształci stan wielofotonowy $|\bar{N}>$ w stan:

$$\begin{aligned} |\bar{N}'> &= \sum_{N=0}^{\infty} \sum_{K=0}^{N} a_N \binom{N}{K} T^K (1-T)^{N-K} |K> = \\ &= \sum_{K=0}^{\infty} \sum_{N=K}^{\infty} a_N \binom{N}{K} T^K (1-T)^{N-K} |K> \end{aligned} \tag{B.4}$$

Dążymy do wyznaczenia współczynników $a_K$' rozwinięcia stanu $|\bar{N}'>$ na stany jednofotonowe:

$$|\bar{N}'> = \sum_{K=0}^{\infty} a_K' |K> \tag{B.5}$$

Porównując (B.5) z (B.4) możemy wyrazić współczynniki $a_K$' przez $a_N$:

$$\begin{aligned} a_K' &= \sum_{N=K}^{\infty} a_N \binom{N}{K} T^K (1-T)^{N-K} = \\ &= \sum_{N=K}^{\infty} \int_0^\infty \frac{(\alpha W)^N}{N!} \mathrm{e}^{-\alpha W} \rho(W;\bar{W}) \frac{N!}{(N-K)!K!} T^K (1-T)^{N-K} \end{aligned} \tag{B.6}$$

Dokonajmy teraz przeindeksowania ($N \to N - K$) oraz zamiany kolejności całkowania i sumowania, a następnie wyeliminujmy z wyrażenia (B.6) sumę po $N$:

$$\begin{aligned} a_K' &= \int_0^\infty \sum_{N=0}^{\infty} (\alpha W)^{N+K} \mathrm{e}^{-\alpha W} \rho(W;\bar{W}) \frac{1}{N!K!} T^K (1-T)^N dW = \\ &= \int_0^\infty \frac{(T\alpha W)^K}{K!} \rho(W;\bar{W}) \sum_{N=0}^{\infty} \frac{[\alpha W(1-T)]^N}{N!} dW = \\ &= \int_0^\infty \frac{(T\alpha W)^K}{K!} \mathrm{e}^{-\alpha W} \rho(W;\bar{W}) \mathrm{e}^{\alpha W(1-T)} dW = \int_0^\infty \frac{(T\alpha W)^K}{K!} \mathrm{e}^{-T\alpha W} \rho(W;\bar{W}) dW \end{aligned} \tag{B.7}$$

Wprowadźmy oznaczenie: *W'* = *TW*, i dokonajmy zamiany zmiennych:

$$a_K' = \int_0^\infty \frac{(\alpha W')^K}{K!} \mathrm{e}^{-\alpha W'} \rho(W;\bar{W}) \frac{dW'}{T} = \int_0^\infty \frac{(\alpha W')^K}{K!} \mathrm{e}^{-\alpha W'} \left[ \frac{1}{T} \rho(W;\bar{W}) \right] dW' \qquad \text{(B.8)}$$

Aby statystyka światła pozostawała niezmieniona po przejściu przez płytkę światłodzielącą wyrażenie okreslające $a_K$' musi mieć taką samą postać jak wyrażenie (8.2), określające $a_N$:

$$a_K' = \int_0^\infty \frac{(\alpha W')^K}{K!} \mathrm{e}^{-\alpha W'} \rho(W';\bar{W}')dW' \qquad \text{(B.9)}$$

Porównanie wyrażeń (B.8) i (B.9) daje warunek (konieczny i dostateczny), aby światło o statystyce opisanej rozkładem $\rho$ nie zmieniało tej statystyki po przejściu przez płytkę światłodzielącą:

$$\begin{gathered} \tfrac{1}{T} \rho(W;\bar{W}) = \rho(W';\bar{W}') \\ \boldsymbol{\rho(W;\bar{W}) = T\rho(TW;T\bar{W})} \end{gathered} \qquad \text{(B.10)}$$

Aby sprawdzić, jakie rozkłady $\rho$ spełniają warunek B.10 dokonam zamiany zmiennych, od których zależy $\rho$, z *W* na *TW* (skorzystam w tym celu ze wzoru na zamiannę zmiennych w rozkładach prawdopodobieństwa, por. [3]):

$$\rho(W';\bar{W}') = \rho(W;\bar{W}) \left| \frac{\mathrm{d}W}{\mathrm{d}W'} \right| = \rho(W;\bar{W}) \frac{1}{T} \qquad \text{(B.11)}$$

A więc $\rho(W;\bar{W}) = T\rho(W';\bar{W}') = T\rho(TW;\bar{W}')$! Sprawdźmy jeszcze jaka jest średnia rozkładu $\rho$(*W'*):

$$\begin{gathered} \bar{W}' = \int_0^\infty W' \rho(W';\bar{W}')dW' = \int_0^\infty \cancel{T}W \frac{1}{\cancel{T}} \rho(W;\bar{W})dW' = \left| \begin{matrix} W'=TW \\ dW'=TdW \end{matrix} \right| = \\ = T\int_0^\infty W\rho(W;\bar{W})dW = T\bar{W} \end{gathered} \qquad \text{(B.12)}$$

Wynik (B.11) i (B.12) oznacza, że $\rho$ spełnia (B.10):

$$\rho(W',\bar{W}') = \tfrac{1}{T} \rho(W,\bar{W})$$

Ponieważ na temat rozkładu $\rho$ nie zostały poczynione żadne założenia (ponad to, że $\rho$ jest rozkładem prawdopodobieństwa), (B.10) jest spełnione dla dowolnego $\rho$. A zatem dla dowolnego stanu światła, *dającego zapisać się jako superpozycja stanów jednofotnowych*, przejście światła przez płytkę światłodzielącą nie spowoduje zmiany statystyki tego stanu.

# CHAPTER 2

# BASIC PRINCIPLE OF PHOTOMULTIPLIER TUBES[1] – [5]

*A photomultiplier tube is a vacuum tube consisting of an input window, a photocathode and an electron multiplier sealed into an evacuated glass tube. Figure 2-1 shows the schematic construction of a photomultiplier tube.*

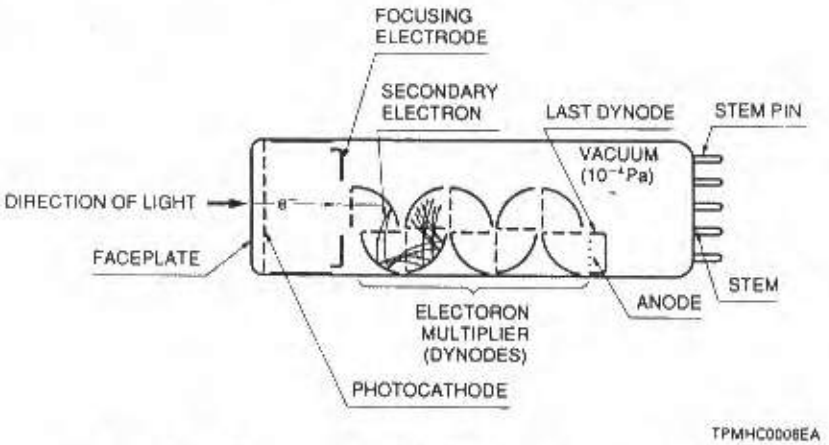


**Figure 2-1: Construction of a photomultiplier tube**

*Light which enters a photomultiplier tube is detected and output as a signal through the following processes.*

*(1) Light passes through the input window.*

*(2) Excites the electrons in the photocathode so that photoelectrons are emitted into the vacuum (external photoelectric effect).*

*(3) Photoelectrons are accelerated and focused by the focusing electrode onto the first dynode where they are multiplied by means of secondary electron emission. This secondary emission is repeated at each of the successive dynodes.*

*(4) The multiplied secondary electrons emitted from the last dynode are finally collected by the anode.*

*This chapter describes the principles of photoelectron emission, electron trajectory, and design and functions of electron multipliers. The electron multipliers used for photomultiplier tubes are classified into two types: normal discrete dynodes consisting of multiple stages and continuous dynodes such as microchannel plates. Since both types of dynodes differ considerably in operating principle, photomultiplier tubes using microchannel plates (MCP-PMTs) are separately described in Chapter 4. Furthermore, electron multipliers intended for use in particle and radiation measurement are discussed in Chapter 5.*

# 2. 1 Photoelectron Emission[6][7]

Photoelectric conversion is broadly classified into external photoelectric effects by which photoelectrons are emitted into the vacuum from a material and internal photoelectric effects by which photoelectrons are excited into the conduction band of a material. The photocathode has the former effect and the latter are represented by the photoconductive or photovoltaic effect.

Since a photocathode is a semiconductor, it can be described using a band model as shown in Figure 2-2.

In a semiconductor band model, there exist a forbidden-band gap or energy gap (EG) that cannot be occupied by electrons, electron affinity (EA) which is an interval between the conduction band and the vacuum level barrier (vacuum level), and work function ( $\phi$ ) which is an energy difference between the Fermi level and the vacuum level. When photons strike a photocathode, electrons in the valence band absorb photon energy (h $\nu$ ) and become excited, diffusing toward the photocathode surface. If the diffused electrons have energy enough to overcome the vacuum level barrier, they are emitted into the vacuum as photoelectrons. This can be expressed in a probability process, and the quantum efficiency $\eta(\nu)$, i.e., the ratio of output electrons to incident photons is given by

$$\eta(\nu) = (1 - R)\frac{P_\nu}{k} \cdot \left(\frac{1}{1 + 1/kL}\right) \cdot Ps$$

where

R : reflection coefficient
k : full absorption coefficient of photons
$P_\nu$ : probability that light absorption may excite electrons to a level greater than the vacuum level
L : mean escape length of excited electrons
Ps : probability that electrons reaching the photocathode surface may be released into the vacuum
$\nu$ : frequency of light

(1) ALKALI PHOTOCATHODE

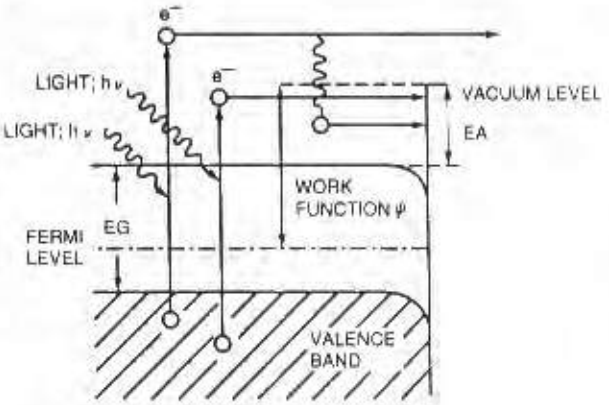


(2) III-V SEMICONDUCTOR PHOTOCATHODE

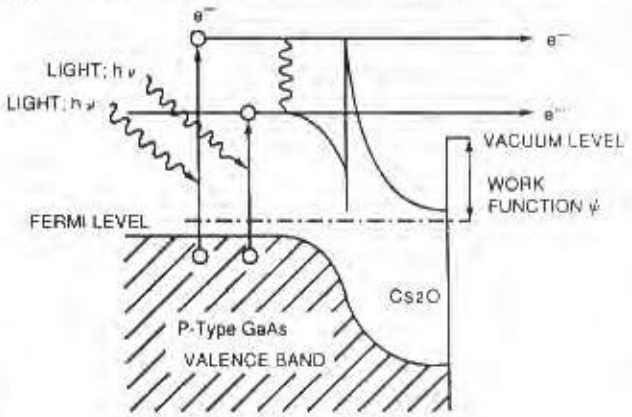


TPMOC3003EA

**Figure 2-2: Photocathode band models**

In the above equation, if we have chosen an appropriate material which determines parameters R, k and $P_\nu$, the factors that dominate the quantum efficiency will be L (mean escape length of excited electrons) and Ps (probability that electrons may be emitted into the vacuum). L becomes longer by use of a better crystal and Ps greatly depends on electron affinity (EA).

Figure 2-2 (2) shows the band model of a photocathode using groups Ⅲ - Ⅴ compound semiconductors[8][10]. If a surface layer of electropositive material such as $Cs_2O$ is applied to this photocathode, a depletion layer is formed, causing the band structure to be bent downward. This bending can make the electron affinity negative. This state is called NEA (negative electron affinity). The NEA effect increases the probability (Ps) that the electrons reaching the photocathode surface may be emitted into the vacuum. In particular, it enhances the quantum efficiency at long wavelengths with lower excitation energy. In addition, it lengthens the mean escape distance (L) of excited electrons due to the depletion layer.

Photocathodes can be classified by photoelectron emission process into a reflection mode and a transmission

mode. The reflection mode photocathode is usually formed on a metal plate, and photoelectrons are emitted in the opposite direction of the incident light. The transmission mode photocathode is usually deposited as a thin film on a glass plate which is optically transparent. Photoelectrons are emitted in the same direction as that of the incident light. (Refer to Figures 2-3, 2-4 and 2-5. ) The reflection mode photocathode is mainly used for the side-on photomultiplier tubes which receive light through the side of the glass bulb, while the transmission mode photocathode is used for the head-on photomultiplier tubes which detect the input light through the end of a cylindrical bulb.

The wavelength of maximum response and long-wavelength cutoff are determined by the combination of alkali metals used for the photocathode and its fabrication process. As an international designation, photocathode sensitivity[11] as a function of wavelength is registered as an "S" number by the JEDEC (Joint Electron Devices Engineering Council). This "S" number indicates the combination of a photocathode and window material and at present, numbers from S-1 through S-25 have been registered. However, other than S-1, S-11, S-20 and S-25 these numbers are scarcely used. Refer to Chapter 3 for the spectral response characteristics of various photocathodes and window materials.

## 2. 2 Electron Trajectory

In order to collect photoelectrons and secondary electrons efficiently on a dynode and also to minimize the electron transit time spread, electrode design must be optimized through an analysis of the electron trajectory[12)-16].

Electron movement in a photomultiplier tube is influenced by the electric field which is dominated by the electrode configuration, arrangement, and also the voltage applied to the electrode. Conventional analysis of the electron trajectory has been performed by simulation models of an actual electrode, using methods such as rubber films and an electrolytic bath. Recently, however, numerical analysis using high-speed, large-capacity computers have come into use. This method divides the area to be analyzed into a grid-like pattern to give boundary conditions, and obtains an approximation by repeating computations until the error converges. By solving the equation for motion based on the potential distribution obtained using this method, the electron trajectory can be predicted.

When designing a photomultiplier tube, the electron trajectory from the photocathode to the first dynode must be carefully designed in consideration of the photocathode shape (planar or spherical window), the shape and arrangement of the focusing electrode and the supply voltage, so that the photoelectrons emitted from the photocathode are efficiently focused onto the first dynode. The collection efficiency of the first dynode is the ratio of the number of electrons landing on the effective area of the first dynode to the number of emitted photoelectrons. This is usually better than 60 to 90 percent. In some applications where the electron

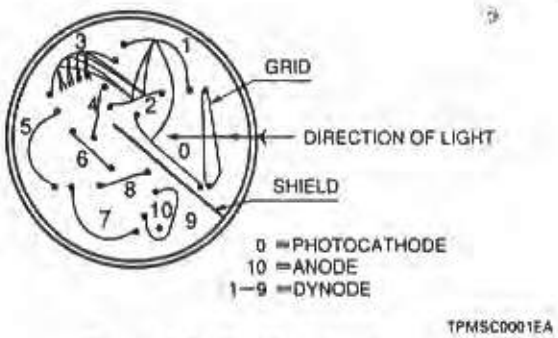


**Figure 2-3: Circular-cage type**

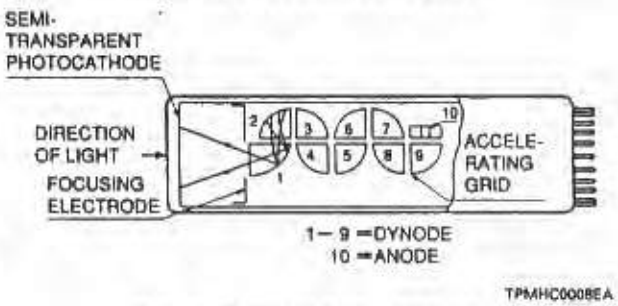


**Figure 2-4: Box-and-grid type**

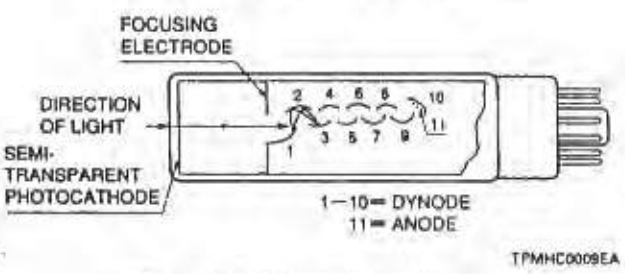


**Figure2-5: Linear-focused type**

transit time needs to be minimized, the electrode should be designed not only for optimum configuration but also for higher electric fields than usual.

The dynode section is usually constructed from several to more than ten stages of secondary-emissive electrodes (dynodes) having a curved surface. To enhance the collection efficiency of each dynode and minimize the electron transit time spread, the optimum configuration and arrangement should be determined from an analysis of the electron trajectory. It is also necessary to design the arrangement of the dynodes in order to prevent ion or light feedback from the latter stages.

In addition, various characteristics of a photomultiplier tube can also be calculated by computer simulation. For example, the collection efficiency, uniformity, and electron transit time can be calculated using a Monte Carlo simulation by setting the initial conditions of photoelectrons and secondary electrons. This allows collective evaluation of photomultiplier tubes. Figures 2-3, 2-4 and 2-5 are cross sections of photomultiplier tubes having a circular-cage, box-and-grid, and linear-focused dynode structures, respectively, showing their typical electron trajectories.

## 2. 3 Electron Multiplier (Dynode Section)

As stated above, the potential distribution and electrode structure of a photomultiplier tube is designed to provide optimum performance. Photoelectrons emitted from the photocathode are multiplied by the first dynode through the last dynode (up to 19th dynode), with current amplification ranging from 10 to as much as $10^8$ times, and are finally sent to the anode.

Major secondary emissive materials[17)-21)] used for dynodes are alkali antimonide, beryllium oxide (BeO), magnesium oxide (MgO), gallium phosphide (GaP) and gallium arsenide phosphied (GaAsP). These materials are coated on a substrate electrode made of nickel, stainless steel, or copper-beryllium alloy. Figure 2-6 shows a model of the secondary emission multiplication of a dynode.

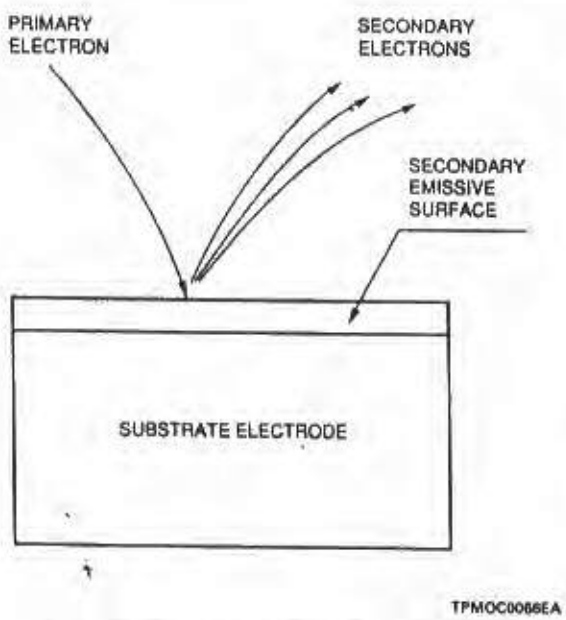


**Figure 2-6: Secondary emission of dynode**

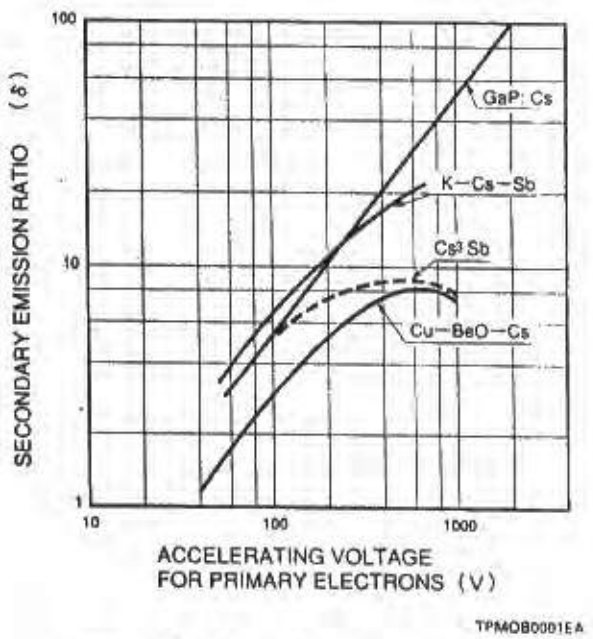


**Figure 2-7: Secondary emission ratio**

When a primary electron with initial energy Ep strikes the surface of a dynode, $\delta$ secondary electrons are emitted. This $\delta$, the number of secondary electrons per primary electron, is called the secondary emission ratio. Figure 2-7 shows the secondary emission ratio $\delta$ for various dynode materials as a function of the accelerating voltage for the primary electrons.

Ideally, the current amplification of a photomultiplier tube having the number of dynode stages n and the average secondary emission ratio $\delta$ per stage will be $\delta^n$. Refer to Section 3.2.2 in Chapter 3 for more details on the current amplification.

Because a variety of dynode structures are available and their current amplification, time response, uniformity, and collection efficiency differ depending on the number of dynode stages and other factors, it is necessary to select the optimum dynode type according to your application. These characteristics are described in Chapter 3, Section 3.2.1.

## References in Chapter 2


1) Hamamatsu Photonics: "Photomultiplier Tubes and Related Products" (1990, October revision)
2) Hamamatsu Photonics: "Characteristics and Uses of Photomultiplier Tubes" No.79-57-03 (1982).
3) S.K. Poultney: Advances in Electronics and Electron Physics 31, 39 (1972). 4)
D.H. Seib and L.W. Ankerman: Advances in Electronics and Electron Physics, 34, 95 (1973).
5) J.P. Boutot, et al.: Advances in Electronics and Electron Physics 60, 223 (1983).
6) T. Hiruma: SAMPE Journal, 24, 6, 35-40 (1988).
7) T. Hayashi: Bunkou Kenkyuu, 22, 233 (1973). (Published in Japanese)
8) H. Sonnenberg: Appl. Phys. Lett., 16, 245 (1970).
9) W.E. Spicer, et al.: Pub. Astrom. Soc. Pacific, 84, 110 (1972).
10) M. Hagino, et al.: Television Journal, 32, 670 (1978). (Published in Japanese)
11) A. Honma: Bunseki, 1, 52 (1982). (Published in Japanese)
12) K.J. Van. Oostrum: Philips Technical Review, 42, 3 (1985).
13) K. Oba and Ito: Advances in Electronics and Electron Physics, 64B, 343.
14) A.M. Yakobson: Radiotekh & Electron, 11, 1813 (1966).
15) H. Bruining: Physics and Applications of Secondary Electron Emission, (1954).
16) J. Rodeny and M. Vaughan: IEEE Transaction on Electron Devices, 36, 9 (1989).
17) B. Gross and R. Hessel: IEEE Transaction on Electrical Insulation, 26, 1 (1991).
18) H.R. Krall, et al.: IEEE Trans. Nucl. Sci. NS-17, 71 (1970).
19) J.S. Allen: Rev. Sci. Instr., 18 (1947).
20) A.M. Tyutikov: Radio Engineering And Electronic Physics, 84, 725 (1963).
21) A.H. Sommer: J. Appl. Phys., 29, 598 (1958).

The polarization that provides the maximum sensitivity is the component perpendicular to the tube axis (P component). In contrast, the polarization that gives the minimum sensitivity is the component parallel to the tube axis (S component), independent of the type of tube and wavelength of incident light. As can be seen from Figure 3-42, this is probably due to a change in the photocathode transmittance. The S component increases in reflectance as the angle of incidence becomes larger, whereas the P component decreases. Moreover, as the wavelength shifts to the longer side, the reflectance generally decreases and the polarization factor P becomes smaller accordingly, as shown in Figure 3-44.

In applications where the polarized-light dependence of a photomultiplier tube cannot be ignored, it will prove effective to place a diffuser such as frosted glass or tracing paper in front of the input window of the photomultiplier tube or to use a photomultiplier tube with a frosted window.

## 3.4 Photon Counting

Photon counting[23][39][43]-[50] is an effective technique used to detect very-low-level-light such as Raman spectroscopy, fluorescence analysis, and chemical or biological luminescence analysis where the absolute magnitude of the light is extremely low. This section describes the principles of photon counting, its operating methods, detection capabilities, and advantages as well as typical characteristics of photomultiplier tubes designed for photon counting.

### 3.4.1 Analog and digital (photon counting) modes

The methods of processing the output signal of a photomultiplier tube can be divided broadly into analog and digital modes, depending on the incident light intensity and the bandwidth of the output processing circuit.

As Figure 3-46 shows, when light strikes the photocathode of a photomultiplier tube, photoelectrons are emitted. These photoelectrons are multiplied by the cascade process of secondary emission through the dynodes (normally $10^6$ to $10^7$ times) and finally reach the anode connecting with an output processing circuit.

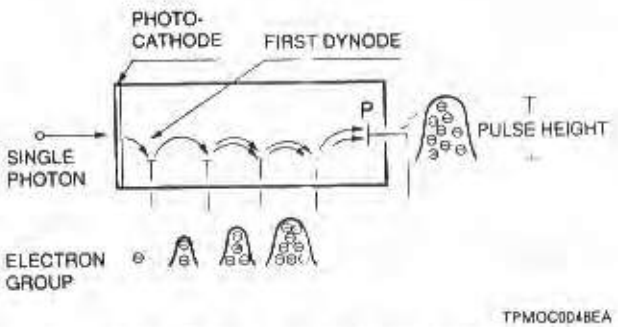


**Figure 3-46: Photomultiplier tube operation in the photon counting mode**

When observing the output signal of a photomultiplier tube with an oscilloscope while varying the incident light level, output pulses like those shown in Figure 3-47 are seen. At higher light levels, the output pulse intervals are narrow so that they overlap each other, producing an analog waveform (similar to (a) and (b) of Figure 3-47). If the light level becomes very low, the ratio of AC component (fluctuation) in the signal increases, and finally the output signal will be discrete pulses (like (c) of Figure 3-47). By discriminating these discrete pulses at a proper binary level, the number of the signal pulses can be counted in a digital mode. This is commonly known as photon counting.

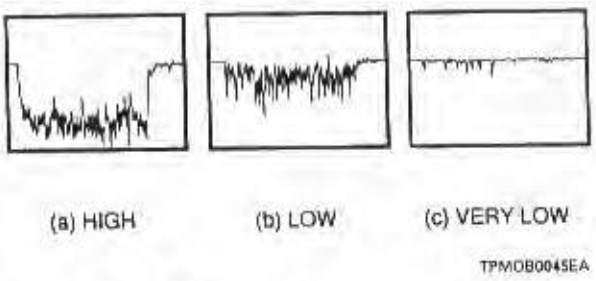


**Figure 3-47: Photomultiplier tube output waveforms observed at different light levels**

In analog mode measurements, the output signal is the mean value of the signals including the AC components shown in Figure 3-47 (a). In contrast,

the photon counting method can detect each pulse shown in Figure 3-47 (c), thus the number of counted pulses equals the signal. This photon counting mode uses a pulse height discriminator that separates the signal pulses from the noise pulses, enabling high-precision measurement with a higher signal-to-noise ratio in comparison with the analog mode. Therefore photon counting is exceptionally effective in detecting low level light.

## 3. 4. 2 Principle of photon counting

When light incident on a photomultiplier tube becomes very low and reaches a state in which no more than two photoelectrons are emitted within the time resolution (pulse width) of the photomultiplier tube, this light level is called the single photoelectron region and photon counting is performed in this region. Quantum efficiency, an important parameter for photon counting, signifies the probability of photoelectron emission when a single photon strikes the photocathode.

In this single photoelectron region, the number of emitted electrons per photon is one or zero and the quantum efficiency can be viewed as the ratio of the number of photoelectrons emitted from the photocathode to the number of incident photons per unit time. The probability that the photoelectrons emitted from the photocathode (primary electrons) will impinge on the first dynode and contribute to current amplification is referred to as collection efficiency. Some photoelectrons may not contribute to current amplification because they deviate from the normal trajectories and are not collected by the first dynode. Additionally, in the photon counting mode, the ratio of the number of counted pulses (output pulses) to the number of incident photons is called detection efficiency or photomultiplier tube counting efficiency and is expressed by the following relation:

$$\text{Detection efficiency (counting efficiency) in the photon counting region} = (Nd/Np) = \eta \times \alpha \quad \text{....(Eq. 3-37)}$$

where Nd is the counted value, Np is the number of incident photons, $\eta$ is the quantum efficiency of the photocathode and $\alpha$ is the collection efficiency of the dynodes. The detection efficiency greatly depends on the threshold level used for binary processing.

The number of secondary electrons released from the first dynode is not constant. It is around several secondary electrons per primary electron, with a broad probability seen as a Poisson distribution. Therefore the average number of electrons per primary electron $\delta$ corresponds to the secondary-electron multiplication factor of the dynode. Similarly, this process is repeated through the second and subsequent dynodes until the final electron bunch reaches the anode. In this way the output multiplied in accordance with the number of photoelectrons from the photocathode appears at the anode. If the photomultiplier tube has n stage dynodes, the photoelectrons emitted from the photocathode are multiplied in cascade up to $\delta^n$ times and derived as an adequate electron bunch from the anode. In this process, each output pulse obtained at the anode exhibits a certain distribution in pulse height because of fluctuations in the secondary multiplication factor at each dynode (statistical fluctuation due to cascade multiplication), non-uniformity of multiplication depending on the dynode position and electrons deviating from their favorable trajectories. Figure 3-48 illustrates a histogram of photomultiplier tube output pulses. The abscissa indicates the pulse height and the anode output pulses are integrated with time. This graph is known as the pulse height distribution.

Figure 3-48 also shows the relation between the pulse height distribution and the actual output pulses obtained with a photomultiplier tube. The pulse height distribution is usually taken with a multichannel analyzer (MCA) frequently used in scintillation counting applications.

Figure 3-49 (a) shows examples of the pulse height distribution obtained with a photomultiplier tube. The output pulses are present even if no light falls on the photomultiplier tube. (These are called dark current pulses or noise pulses.) The broken line indicates the distribution of the dark current pulses, with a tendency to build up somewhat in the lower pulse height region (left side). These dark pulses mainly originate from the thermal electron emission at the photocathode and also at the dynodes. The thermal electrons from the dynodes are multiplied less than those from the photocathode and are therefore distributed in the lower pulse height region.

Figure 3-49 (b) indicates the distribution of the total number of counted pulses S(L) with amplitudes greater than a threshold level L shown in (a). (a) and (b) have differential and integral relations to each other. Item (b) is a typical integral curve taken with a photon counting system using a photomultiplier tube.

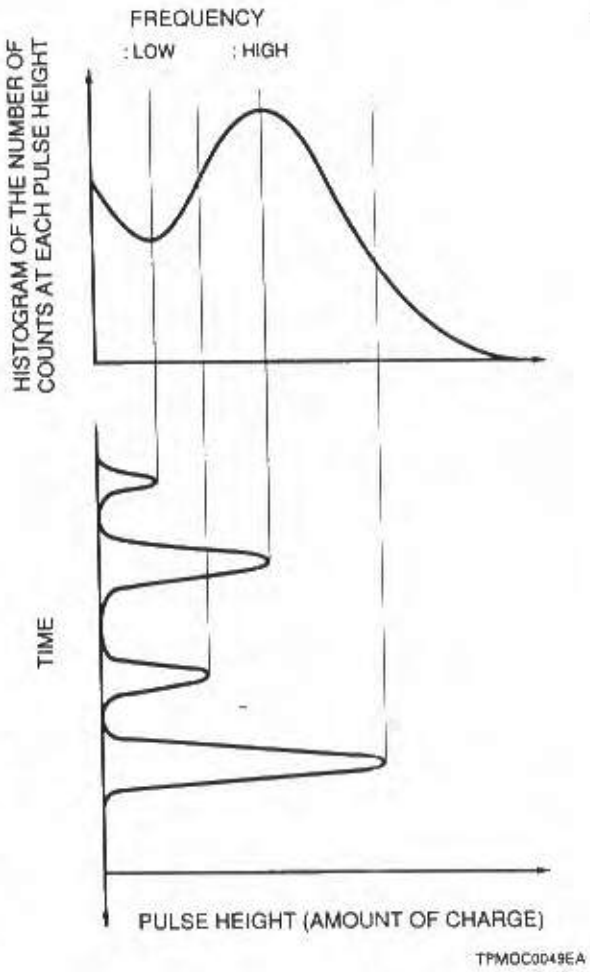


**Figure 3-48: Photomultiplier tube output and its pulse height distribution**

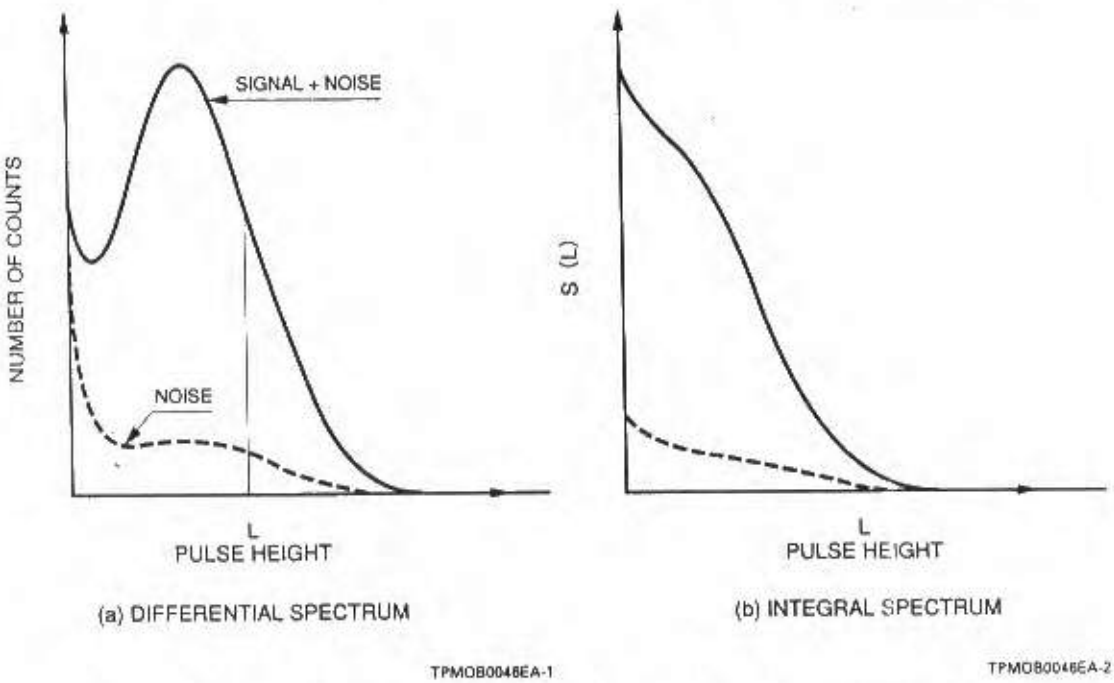


**Figure 3-49: Differential and integral representations of pulse height distribution**

## 3. 4. 3 Operating method and characteristics for photon counting

This section discusses specific circuit configurations used to perform photon counting and the basic characteristics involved in photon counting.

### (1) Circuit configuration

Figure 3-50 shows a typical circuit configuration for photon counting and a pulse waveform obtained at each circuit.

(a) Using a counter

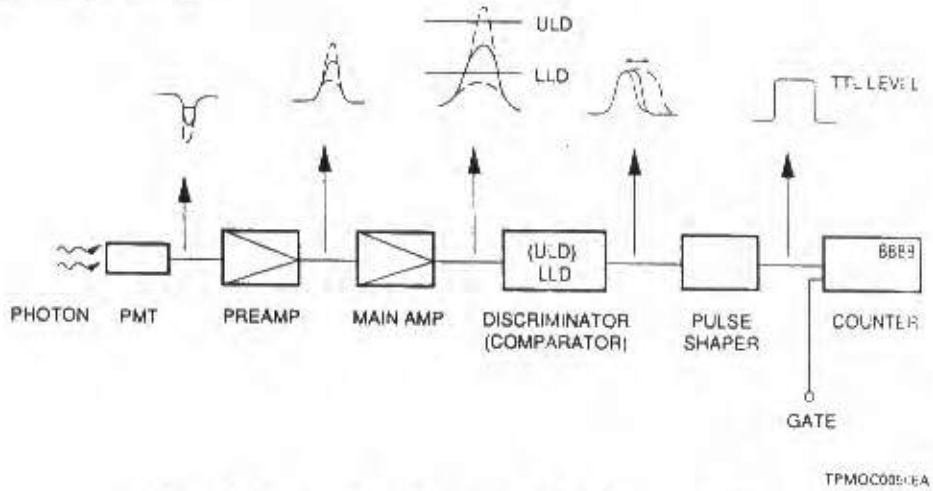


**Figure 3-50: Circuit configuration for photon counting**

In the above system, current output pulses from a photomultiplier tube are converted to a voltage by a wide-band preamplifier and amplified. These voltage pulse are fed to a discriminator and then to a pulse shaper. Finally the number of pulses is counted by a counter. The discriminator usually employs a comparator IC that compares the input voltage pulses with the preset reference voltage (threshold level) and eliminates those pulses with amplitudes lower than this value. In general, the LLD (lower level discrimination) level is set at the lower pulse height side. The ULD (upper level discrimination) level may also be often set at the higher pulse height side to eliminate noise pulses with higher amplitudes. The counter is usually equipped with a gate circuit, allowing measurement at different timings and intervals.

### (2) Basic characteristics in photon counting

#### *a) Pulse height distribution and plateau characteristics*

Figure 3-51 illustrates a typical pulse height distribution obtained by photon counting. The plot with a high peak shows the pulse height distribution for signal pulses, and the lower plot shows that for noise pulses.

If a multichannel pulse height analyzer is available, a proper threshold level can be set in the pulse height distribution. Because the dark current pulses are usually distributed in the lower pulse height region, setting the LLD level in the vicinity of the valley ($L_v$) of the distribution can effectively eliminate such noise pulses without sacrificing the detection efficiency. In actual operation, however, using a pulse height analyzer is not so popular. Other methods using plateau characteristics are more commonly employed instead. By

counting the total number of pulses with amplitudes higher than the preset threshold level while varying the supply voltage for the photomultiplier tube, plots similar to those shown in Figure 3-52 can be obtained. These plots are called the plateau characteristics. The pulse height obtained at the supply voltage giving the maximum rising gradient in the signal plateau characteristic corresponds to the L1 level in Figure 3-51. From this relation, the pulse height for the LLD level can be predicted.

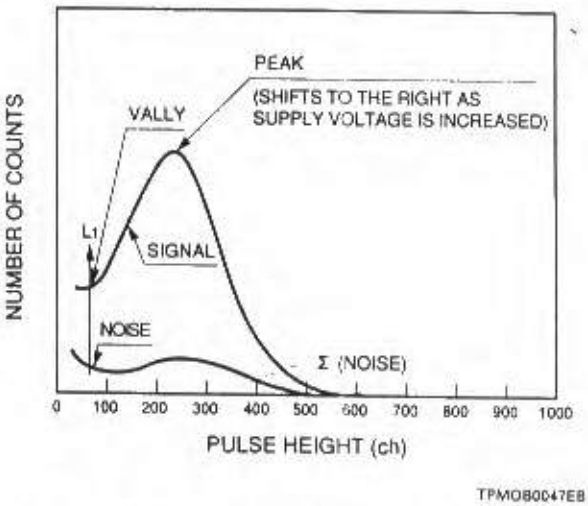


**Figure 3-51: Typical example of pulse height distribution**

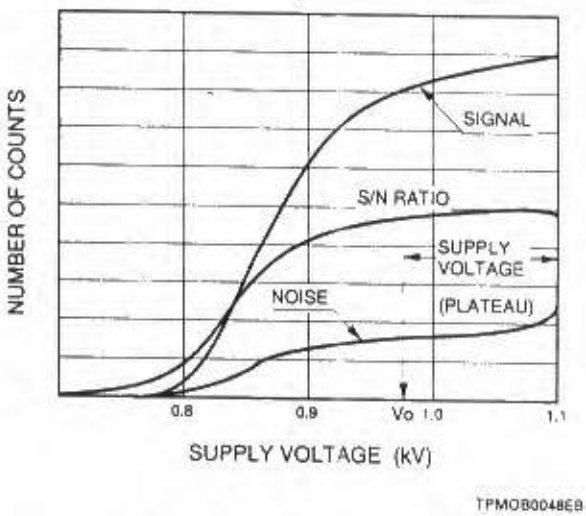


**Figure 3-52: Plateau characteristics**

### *b) Setting the photomultiplier tube supply voltage*

The signal-to-noise ratio is an important factor from the viewpoint of accurate measurements. Here the signal-to-noise ratio is defined as the ratio of the mean value of the signal count rate to the fluctuation of the counted signal and noise pulses (expressed in standard deviation or root mean square). The signal-to-noise ratio curve shown in Figure 3-52 is plotted by varying the supply voltage, the same procedure which is used to obtain the plateau characteristics. This figure implies that the photomultiplier tube should be operated in the range between the voltage (Vo) at which the plateau region begins and the maximum supply voltage.

### c) Linearity of the count rate

The photon counting mode offers excellent linearity over a wide range. The lower limit of the count rate linearity is determined by the number of dark current pulses, and the upper limit by the maximum count rate. The maximum count rate further depends on pulse-pair resolution, which is the minimum time interval at which each pulse can be separated. The reciprocal of this pulse pair resolution would be the maximum count rate. However, since most events in the photon counting region usually occur at random, the counted pulses may possibly overlap. Considering this probability of overlapping, the actual maximum count rate will be about one-tenth of the calculated above. The loss of count rate $\xi$ from pulse overlapping is given by

$$\xi = \frac{n\tau}{1 + n\tau} \quad \text{..... (Eq. 3-38)}$$

where

n : true count rate (cps)
τ : pulse pair resolution (s)

Figure 3-53 shows the typical linearity taken using a system with a pulse pair resolution of 8 nanoseconds.

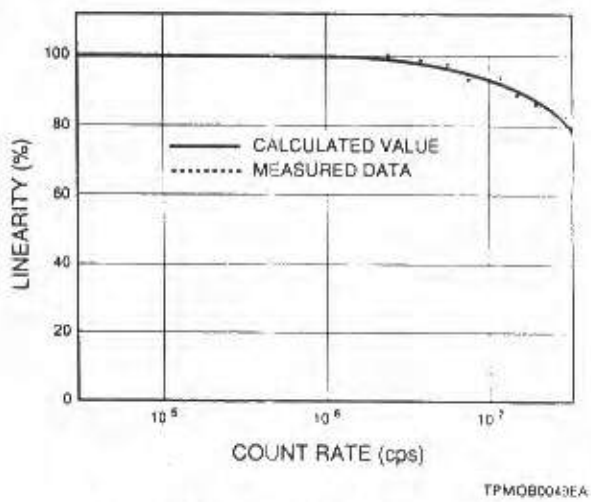


**Figure 3-53: Linearity of count rate**

### d) Setting the threshold level

In photon counting, it is most important to determine where to set the threshold level. In general, the optimum threshold level may be determined according to the suggestions listed below. But setting threshold is not simple and therefore careful selection must be made in accordance with individual needs.

① To optimize the signal-to-noise ratio and stabilize the count rate with respect to gain variations of the photomultiplier tube, the threshold level should be set near the valley or the plateau region of the pulse height distribution.

② Setting the threshold level at the lowest possible level gives the best detection efficiency. Practically, however, setting it near the valley or the plateau region is recommended.

③ To optimize the elimination rate between the signal and noise, the threshold level should be set at the middle of the peak and valley in the pulse height distribution.

### e) *Advantages of photon counting*

Photon counting has many advantages in comparison with the analog mode. Among them, stability and signal-to-noise ratio are discussed in this section.

#### ( I ) Stability

One of the significant advantages photon counting offers is operating stability. The photon counting mode is resistant to variations in supply voltage and photomultiplier tube gain. If the supply voltage is set within the plateau region, a change in the voltage has less effect on the output counts. In the analog mode, however, it affects the output current considerably. Immunity to variations in the supply voltage means that the photon counting mode also assures high stability against gain fluctuation of the photomultiplier tube. Normally the photon counting mode offers several times higher immunity to such variations than the analog mode. (Refer to Figure 3-54.)

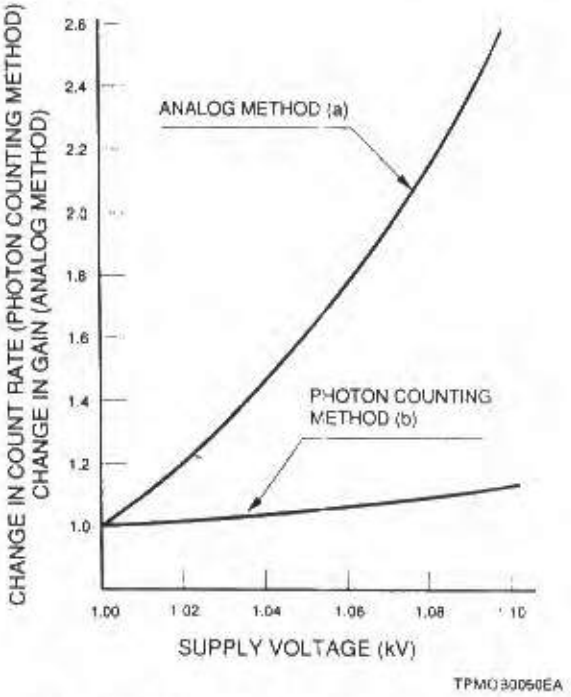


**Figure 3-54: Stability versus changes in supply voltage**

#### ( II ) Signal-to-noise ratio

When signal light strikes the photocathode of a photomultiplier tube, photoelectrons are emitted and directed to the dynode section where secondary electrons are produced. The number of photoelectrons produced per unit time and also the number of secondary electrons produced are determined by statistical probability of events which is represented by a Poisson distribution. Thus they are accompanied by statistical fluctuations (AC current components) expressed as a binomial distribution, having an effect on the signal-to-noise ratio. The signal-to-noise ratio is also described in Section 3.3.7. The AC component noise which is superimposed on the signal can be categorized by origin as follows

① Shot noise resulting from signal light
② Shot noise resulting from background light
③ Shot noise resulting from dark current

In the analog mode, the signal-to-noise ratio[39)40)43)45)–48)50)] of the photomultiplier tube output including these shot noises becomes

$$\text{S/N ratio (current)} = \frac{\text{Iph}}{\sqrt{2\text{eNFB}\left\{\text{Iph} + 2\,(\text{Ib} + \text{Id})\right\}}} \quad \text{.....(Eq. 3-39)}$$

where

Iph: signal current produced by incident light (A)
e : electron charge (c)
NF: noise figure of the photomultiplier tube

Ib : cathode current resulting from background light
Id : cathode current resulting from dark current (A)
B : Bandwidth of measurement system (Hz)

Here the true signal current Iph is obtained by subtracting Ib+Id from the total current. The noise originating from the latter-stage amplifier is considered to be negligible because the typical current amplification $\mu$ of a photomultiplier tube is sufficiently large.

The signal-to-noise ratio in the photon counting mode is given by the following equation.

$$\text{S/N ratio} = \frac{Ns\sqrt{T}}{\sqrt{Ns + 2\,(Nb + Nd)}} \quad \text{.....(Eq. 3-40)}$$

where

Ns : number of counts/sec resulting from incident light per second
Nb : number of counts/sec resulting from background light per second
Nd : number of counts/sec resulting from dark current per second
T : measurement time (sec)

Here the number of counts /sec of true signals Ns is obtained by subtracting Nb+Nd from the total number of counts.

From the common equivalent relation between the time and frequency, if B=1 (Hz) and T=0.5 (sec), then the signal-to-noise ratio will be as follows:

in the analog mode

$$\text{S/N ratio (current)} = \frac{Iph}{\sqrt{2eNF\left\{Iph + 2\,(Ib + Id)\right\}}} \quad \text{.....(Eq. 3-41)}$$

in the photon counting mode

$$\text{S/N ratio} = \frac{Ns}{\sqrt{2\left\{Ns + 2\,(Nb + Nd)\right\}}} \quad \text{.....(Eq. 3-42)}$$

Through the above analysis, it is understood that the photon counting mode provides a better signal-to-noise ratio by a factor of the noise figure NF. Since the dark current includes thermal electrons emitted from the dynodes in addition to those from the photocathode, its pulse height distribution will be an exponential spectrum shifted toward the lower pulse height side. Therefore, the dark current component can be effectively eliminated by use of a pulse height discriminator while maintaining the signal component, assuring further improvement in the signal-to-noise ratio. In addition, because only AC pulses are counted, the photon counting mode is not influenced by the DC leakage current. Amplifier noises can totally be eliminated by a discriminator.

CHAPTER

# 11

# PHOTON OPTICS



**Max Planck (1858–1947)** suggested that the emission and absorption of light by matter occur in quanta of energy.

**Albert Einstein (1879–1955)** advanced the hypothesis that light itself consists of quanta of energy.

B. E. A. Saleh, M. C. Teich, "Fundamentals of Photonics", Wiley, New York 1991.

Electromagnetic optics (Chap. 5) provides the most complete treatment of light within the confines of **classical optics**. It encompasses wave optics, which in turn encompasses ray optics (Fig. 11.0-1). Although classical electromagnetic theory is capable of providing explanations for a great many effects in optics, as attested to by the earlier chapters in this book, it nevertheless fails to account for certain optical phenomena. This failure, which became evident about the turn of this century, ultimately led to the formulation of a quantum electromagnetic theory known as **quantum electrodynamics**. For optical phenomena, this theory is also referred to as **quantum optics**. Quantum electrodynamics (QED) is more general than classical electrodynamics and it is today accepted as a theory that is useful for explaining virtually all known optical phenomena.

In the framework of QED, the electric and magnetic fields **E** and **H** are mathematically treated as operators in a vector space. They are assumed to satisfy certain operator equations and commutation relations that govern their time dynamics and their interdependence. The equations of QED are required to accurately describe the interactions of electromagnetic fields with matter in the same way that Maxwell's equations are used in classical electrodynamics. The use of QED can lead to results that are characteristically quantum in nature and cannot be explained classically.

The formal treatment of QED is beyond the scope of this book. Nevertheless, it is possible to derive many of the quantum-mechanical properties of light and its interaction with matter by supplementing electromagnetic optics with a few simple relationships drawn from QED that represent the corpuscularity, localization, and fluctuations of electromagnetic fields and energy. This set of rules, which we call **photon optics**, permits us to deal with optical phenomena that are beyond the reach of classical theory, while retaining classical optics as a limiting case. However, photon optics is not intended to be a theory that is capable of providing an explanation for all optical effects.

In Sec. 11.1 we introduce the concept of the photon and its properties in the form of a number of rules that govern the behavior of photon energy, momentum, polarization, position, time, and interference. These rules take the form of deceptively simple relationships with far-reaching consequences. This is followed, in Sec. 11.2, by a

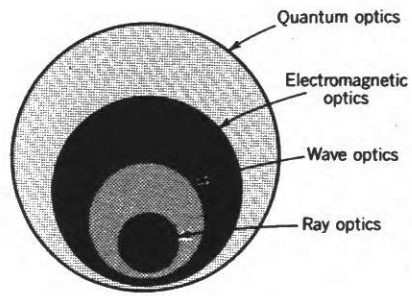


**Figure 11.0-1** The theory of quantum optics provides an explanation for virtually all optical phenomena. It is more general than electromagnetic optics, which was shown earlier to encompass wave optics and ray optics.

discussion of the properties of photon streams. The number of photons emitted by a light source in a given time is almost always random, with statistical properties that depend on the nature of the source. The photon-number statistics for several important optical sources, including the laser and thermal radiators, are discussed. The effects of simple optical components (such as a beamsplitter and a filter) on the randomness of a photon stream are also examined. In Sec. 11.3 we use quantum optics to discuss the random fluctuations of the magnitude and phase of the electromagnetic field and to provide a brief introduction to coherent and squeezed states of light. The interaction of photons with atoms is discussed in Chap. 12.

## 11.1 THE PHOTON

Light consists of particles called **photons**. A photon has zero rest mass and carries electromagnetic energy and momentum. It also carries an intrinsic angular momentum (or spin) that governs its polarization properties. The photon travels at the speed of light in vacuum ($c_o$); its speed is retarded in matter. Photons also have a wavelike character that determines their localization properties in space and the rules by which they interfere and diffract.

The notion of the photon initially grew out of an attempt by Planck to resolve a long-standing riddle concerning the spectrum of blackbody radiation. He finally achieved this goal by quantizing the allowed energy values of each of the electromagnetic modes in a cavity from which radiation was emanating (this subject is discussed in Chap. 12). The concept of the photon and the rules of photon optics are introduced in this section by considering light inside an optical resonator (a cavity). This is a convenient choice because it restricts the space under consideration to a simple geometry. The presence of the resonator turns out not to be an important restriction in the argument; the results can be shown to be independent of its presence.

### *Electromagnetic-Optics Theory of Light in a Resonator*

In accordance with electromagnetic optics, light inside a lossless resonator of volume $V$ is completely characterized by an electromagnetic field that takes the form of a sum of discrete orthogonal modes of different frequencies, different spatial distributions, and different polarizations. The electric field vector is $\mathscr{E}(\mathbf{r}, t) = \mathrm{Re}\{\mathbf{E}(\mathbf{r}, t)\}$, where

$$\mathbf{E}(\mathbf{r}, t) = \sum_{\mathbf{q}} A_{\mathbf{q}} U_{\mathbf{q}}(\mathbf{r}) \exp(j2\pi\nu_{\mathbf{q}} t)\hat{\mathbf{e}}_{\mathbf{q}}. \tag{11.1-1}$$

The $q$th mode has complex amplitude $A_{\mathbf{q}}$, frequency $\nu_{\mathbf{q}}$, polarization along the direction of the unit vector $\hat{\mathbf{e}}_{\mathbf{q}}$, and a spatial distribution characterized by the complex function $U_{\mathbf{q}}(\mathbf{r})$, which is normalized such that $\int_V |U_{\mathbf{q}}(\mathbf{r})|^2 \, d\mathbf{r} = 1$. The choice of the expansion functions $U_{\mathbf{q}}(\mathbf{r})$ and $\hat{\mathbf{e}}_{\mathbf{q}}$ is not unique.

In a cubic resonator of dimension $d$, one convenient choice of the spatial expansion functions is the set of standing waves

$$U_{\mathbf{q}}(\mathbf{r}) = \left(\frac{2}{d}\right)^{3/2} \sin\frac{q_x \pi x}{d} \sin\frac{q_y \pi y}{d} \sin\frac{q_z \pi z}{d}, \tag{11.1-2}$$

where $q_x$, $q_y$, and $q_z$ are integers denoted collectively by the index $\mathbf{q} = (q_x, q_y, q_z)$ [see Sec. 9.1 and Fig. 11.1-1(*a*)]. The energy contained in the mode is

$$E_{\mathbf{q}} = \tfrac{1}{2}\epsilon \int_V \mathbf{E}(\mathbf{r}, t) \cdot \mathbf{E}^*(\mathbf{r}, t) \, d\mathbf{r} = \tfrac{1}{2}\epsilon |A_{\mathbf{q}}|^2.$$



In classical electromagnetic theory, the energy $E_{\mathbf{q}}$ can assume an arbitrary nonnegative value, no matter how small. The total energy is the sum of the energies in all the modes.

### *Photon-Optics Theory of Light in a Resonator*

The electromagnetic-optics theory described above is maintained in photon optics, but a restriction is placed on the energy that is allowed to be carried by each mode. Rather than assuming a continuous range, the energy of a mode is restricted to a discrete set of values equally separated by a fixed energy. The energy of a mode is said to be quantized, with only integral units of this fixed energy allowed. Each unit of energy is carried by a photon.

**Light in a resonator is comprised of a set of modes, each containing an integral number of identical photons. Characteristics of the mode, such as its frequency, spatial distribution, direction of propagation, and polarization, are assigned to the photon.**

### A. Photon Energy

Photon optics provides that the energy of an electromagnetic mode is quantized to discrete levels separated by the energy of a photon (Fig. 11.1-1). The energy of a photon in a mode of frequency $\nu$ is

$$\boxed{E = h\nu = \hbar\omega,} \tag{11.1-3}$$

Photon Energy

where $h = 6.63 \times 10^{-34}$ J-s is **Planck's constant** and $\hbar \equiv h/2\pi$. Energy may be added to, or taken from, this mode only in units of $h\nu$.

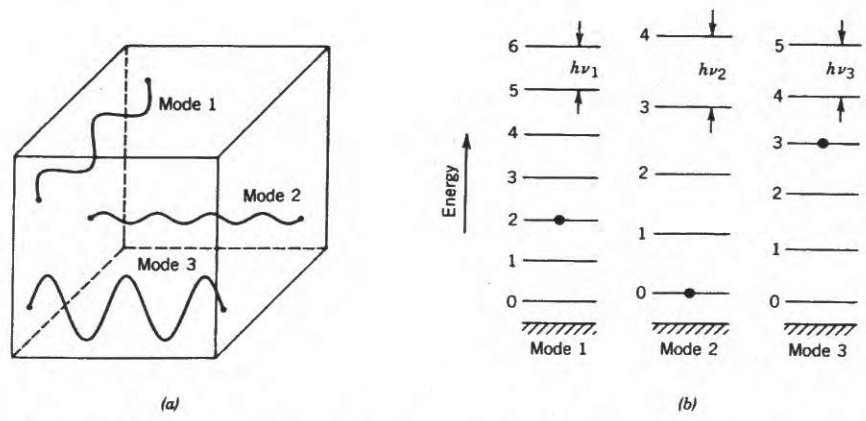


**Figure 11.1-1** (*a*) Three modes of different frequencies and directions in a cubic resonator. (*b*) Allowed energies of three modes of frequencies $\nu_1$, $\nu_2$, and $\nu_3$. The solid circles indicate the number of photons in each mode; modes 1, 2, and 3 contain 2, 0, and 3 photons, respectively.

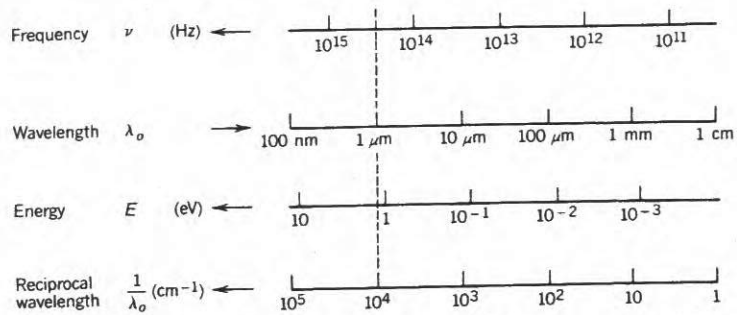


**Figure 11.1-2** Relationships between photon frequency $\nu$ (Hz), wavelength $\lambda_o$, energy $E$ (eV), and reciprocal wavelength $1/\lambda_o$ ($cm^{-1}$). A photon of wavelength 1 cm has reciprocal wavelength 1 $cm^{-1}$. A photon of frequency $\nu = 3 \times 10^{14}$ Hz has wavelength $\lambda_o = 1$ $\mu$m, energy 1.24 eV, and reciprocal wavelength 10,000 $cm^{-1}$.

A mode containing zero photons nevertheless carries an energy $E_0 = \frac{1}{2}h\nu$, which is called the zero-point energy. When it carries $n$ photons, therefore, the mode has total energy

$$E_n = (n + \tfrac{1}{2})h\nu, \qquad n = 0, 1, 2, \ldots . \tag{11.1-4}$$

In most experiments the zero-point energy is not directly observable because only energy differences [such as $E_{n2} - E_{n1}$ in (11.1-4)] are measured. The presence of the zero-point energy can, however, be manifested in subtle ways when matter is exposed to static fields. It plays a crucial role in the process of spontaneous emission from an atom, as discussed in Chap. 12.

The order of magnitude of photon energy is easily estimated. An infrared photon of wavelength $\lambda_o = 1$ $\mu$m has frequency $3 \times 10^{14}$ Hz since $\lambda_o \nu = c_o$ in vacuum. Its energy is thus $h\nu = 1.99 \times 10^{-19}$ J = 1.24 eV (electron volts), which is the same as the kinetic energy of an electron that has been accelerated through a potential difference of 1.24 V. The conversion formula between wavelength ($\mu$m) and photon energy (eV) is therefore simply $\lambda_o(\mu\text{m}) = 1.24/E(\text{eV})$.

As another example, a microwave photon with a wavelength of 1 cm has an energy that is $10^4$ times smaller, $h\nu = 1.24 \times 10^{-4}$ eV. The reciprocal wavelength is often also used as a unit of energy. It is specified in $cm^{-1}$, also called wavenumbers (1 $cm^{-1}$ corresponds to $1.24 \times 10^{-4}$ eV and 1 eV corresponds to 8068.1 $cm^{-1}$). The relationship between photon frequency, wavelength, energy, and reciprocal wavelength is illustrated in Fig. 11.1-2.

Because photons of higher frequency carry larger energy, the particle nature of light becomes increasingly important as the frequency of the radiation increases. Furthermore, wavelike effects such as diffraction and interference become more difficult to discern as the wavelength becomes shorter. X-rays and gamma-rays almost always behave like collections of particles, in contrast to radio waves, which almost always behave like waves. The frequency of light in the optical region is such that both particle-like and wavelike behavior occur, thus spurring the need for photon optics.

## B. Photon Position

Associated with each photon is a wave described by the complex wavefunction $AU(\mathbf{r})\exp(j2\pi\nu t)\hat{\mathbf{e}}$ of the mode. However, when a photon impinges on a detector of small area $dA$ located normal to the direction of propagation at the position $\mathbf{r}$, its



indivisibility causes it to be either wholly detected or not detected at all. The location at which the photon is registered is not precisely determined. It is governed by the optical intensity $I(\mathbf{r}) \propto |U(\mathbf{r})|^2$, in accordance with the following probabilistic law:

The probability $p(\mathbf{r})\,dA$ of observing a photon at a point $\mathbf{r}$ within an incremental area $dA$, at any time, is proportional to the local optical intensity $I(\mathbf{r}) \propto |U(\mathbf{r})|^2$, i.e.,

$$p(\mathbf{r})\,dA \propto I(\mathbf{r})\,dA. \tag{11.1-5}$$

Photon Position

The photon is more likely to be found at those locations where the intensity is high. A photon in a mode described by a standing wave with the intensity distribution $I(x, y, z) \propto \sin^2(\pi z/d)$, where $0 \le z \le d$, for example, is most likely to be detected at $z = d/2$, but will never be detected at $z = 0$ or $z = d$. In contrast to waves, which are extended in space, and particles, which are localized, optical photons behave as extended *and* localized entities. This behavior is called **wave–particle duality**. The localized nature of photons becomes evident when they are detected.

### *EXERCISE 11.1-1*

#### *Photons in a Gaussian Beam*

(a) Consider a single photon described by a Gaussian beam (i.e., a $\text{TEM}_{0,0}$ mode of a spherical-mirror resonator; see Secs. 3.1B, 5.4A, and 9.2B). What is the probability of detecting the photon at a point within a circle whose radius is the waist radius of the beam $W_0$? Recall that at the waist ($z = 0$), $I(\rho, z = 0) \propto \exp(-2\rho^2/W_0^2)$, where $\rho$ is the radial coordinate.

(b) If the beam carries a large number $N$ of independent photons, estimate the average number of photons that lie within this circle.

#### *Transmission of a Single Photon Through a Beamsplitter*

An ideal beamsplitter is an optical device that losslessly splits a beam of light into two beams emerging at right angles. It is characterized by a transmittance $\mathcal{T}$ and a reflectance $\mathcal{R} = 1 - \mathcal{T}$. The intensity of the transmitted wave $I_t$ and the intensity of the reflected wave $I_r$ can be calculated from the intensity of the incident wave $I$ using the electromagnetic relations $I_r = (1 - \mathcal{T})I$ and $I_t = \mathcal{T}I$.

Because a photon is indivisible, it must choose between the two possible directions permitted by the beamsplitter. A single photon incident on it follows one of the two possible paths in accordance with the probabilistic photon-position rule (11.1-5). The probability that the photon is transmitted is proportional to $I_t$ and is therefore equal to the transmittance $\mathcal{T}$. The probability that it is reflected is $1 - \mathcal{T}$. From a probability point of view, the problem is identical to that of flipping a coin. Figure 11.1-3 illustrates the process.

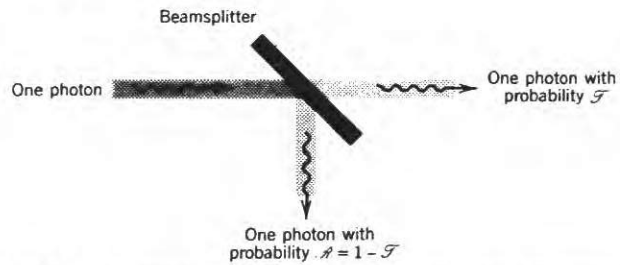


**Figure 11.1-3** Probabilistic reflection or transmission of a photon at a beamsplitter.

## C. Photon Momentum

The momentum of a photon is related to the wavevector of its associated wavefunction by the following rule:

A photon in a mode described by the plane wave

$$\mathbf{E}(\mathbf{r}, t) = A \exp(-j\mathbf{k} \cdot \mathbf{r}) \exp(j2\pi\nu t)\hat{\mathbf{e}}$$

has a momentum vector

$$\mathbf{p} = \hbar\mathbf{k}, \tag{11.1-6}$$

The photon travels in the direction of the wavevector and the magnitude of the momentum is $p = \hbar k = \hbar 2\pi/\lambda$, i.e.,

$$p = \frac{h}{\lambda}. \tag{11.1-7}$$

Electromagnetic optics leads to the same energy–momentum relationship $\mathbf{p} = (E/c)\hat{\mathbf{k}}$ for a plane wave, where $p$ is the momentum content per unit volume of the wave, $E$ is the energy content per unit volume, and $\hat{\mathbf{k}}$ is a unit vector in the direction of $\mathbf{k}$. Of course, the concept of the photon does not exist in electromagnetic optics, so that the expressions in (11.1-6) and (11.1-7) containing $\hbar$ are unique to photon optics.

### *Momentum of a Localized Wave

A wave more general than a plane wave, with a complex wavefunction of the form $AU(\mathbf{r}) \exp(j2\pi\nu t)\hat{\mathbf{e}}$, can be expanded as a sum of plane waves of different wavevectors by using the techniques of Fourier optics (see Chap. 4). The component with wavevector $\mathbf{k}$ may be written in the form $A(\mathbf{k}) \exp(-j\mathbf{k} \cdot \mathbf{r}) \exp(j2\pi\nu t)\hat{\mathbf{e}}$, where $A(\mathbf{k})$ is its amplitude.

The momentum of a photon described by an arbitrary complex wavefunction $AU(\mathbf{r}) \exp(j2\pi\nu t)\hat{\mathbf{e}}$ is uncertain. It has the value

$$\mathbf{p} = \hbar\mathbf{k},$$

with probability proportional to $|A(\mathbf{k})|^2$, where $A(\mathbf{k})$ is the amplitude of the plane-wave Fourier component of $U(\mathbf{r})$ with wavevector $\mathbf{k}$.



If $f(x, y) = U(x, y, 0)$ is the complex amplitude at the $z = 0$ plane, the plane-wave Fourier component of wavevector $\mathbf{k} = (k_x, k_y, k_z)$ has an amplitude $A(\mathbf{k}) = F(k_x/2\pi, k_y/2\pi)$, where $F(\nu_x, \nu_y)$ is the two-dimensional Fourier transform of $f(x, y)$ (see Chap. 4). Because the functions $f(x, y)$ and $F(\nu_x, \nu_y)$ are a Fourier transform pair, their widths are inversely related and satisfy the duration–bandwidth relation (see Appendix A, (A.2-6)). The uncertainty relation between the position of the photon and the direction of its momentum is established because the position of the photon at the $z = 0$ plane is probabilistically determined by $|U(\mathbf{r})|^2 = |f(x, y)|^2$, and the direction of its momentum is probabilistically determined by $|A(\mathbf{k})|^2 = |F(k_x/2\pi, k_y/2\pi)|^2$. Thus if, at the plane $z = 0$, $\sigma_x$ is the position uncertainty in the $x$ direction, and $\sigma_\theta = \sin^{-1}(\sigma_{kx}/k) \approx (\lambda/2\pi)\sigma_{kx}$ is the angular uncertainty about the $z$ axis (assumed $\ll 1$), then the uncertainty relation $\sigma_x\sigma_{kx} \geq \frac{1}{2}$ is equivalent to $\sigma_x\sigma_\theta \geq \lambda/4\pi$.

A plane-wave photon has a known momentum (fixed direction and magnitude), so that $\sigma_\theta = 0$, but its position is totally uncertain ($\sigma_x = \infty$); it is equally likely to be detected anywhere in the $z = 0$ plane. When a plane-wave photon passes through an aperture, its position is localized, at the expense of a spread in the direction of its momentum. The position–momentum uncertainty therefore parallels the theory of diffraction described in Chap. 4. At the other extreme from the plane wave is the spherical-wave photon. It is well localized in position (at the center of the wave), but its momentum has a direction that is totally uncertain.

### Radiation Pressure

Because momentum is conserved, its association with a photon means that the emitting atom experiences a recoil of magnitude $h\nu/c$. Furthermore, the momentum associated with a photon can be transferred to objects of finite mass, giving rise to a force and causing mechanical motion. As an example, light beams can be used to deflect atomic beams traveling perpendicular to the photons. The term **radiation pressure** is often used to describe this phenomenon (pressure is force/area).

### EXERCISE 11.1-2

***Photon-Momentum Recoil.*** Calculate the recoil velocity imparted to a $^{198}$Hg atom that has emitted a photon of energy 4.88 eV. Compare this with the root-mean-square thermal velocity $v$ of the atom at $T = 300$ K (obtained by setting the average kinetic energy equal to the average thermal energy, $\frac{1}{2}mv^2 = \frac{3}{2}k_BT$).

## D. Photon Polarization

As indicated earlier, light is characterized as a sum of modes of different frequencies, directions, and polarizations.

*The polarization of a photon is that of its mode.*

The choice of a particular set of modes is not unique, however. This important concept is best explained by examining the polarization properties of light from the perspective of photon optics.

### Linearly Polarized Photons

Consider light described by a superposition of two plane-wave modes propagating in the $z$ direction, one linearly polarized in the $x$ direction and the other linearly

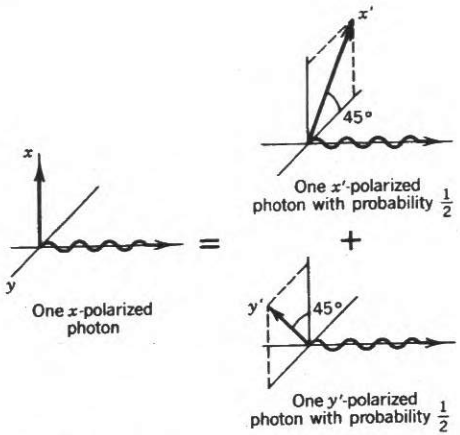


**Figure 11.1-4** Probabilistic outcomes for a linearly polarized photon.

polarized in the $y$ direction:

$$\mathbf{E}(\mathbf{r},t) = (A_x\hat{\mathbf{x}} + A_y\hat{\mathbf{y}})\exp(-jkz)\exp(j2\pi\nu t).$$

However, the very same electromagnetic field may also be represented in a different coordinate system $(x', y')$ (e.g., one that makes a 45° angle with the initial coordinate system). Thus we can equally well view the field in terms of two modes carrying photons polarized along the $x'$ and $y'$ directions, i.e.,

$$\mathbf{E}(\mathbf{r},t) = (A_{x'}\hat{\mathbf{x}}' + A_{y'}\hat{\mathbf{y}}')\exp(-jkz)\exp(j2\pi\nu t),$$

where

$$A_{x'} = \frac{1}{\sqrt{2}}(A_x - A_y), \qquad A_{y'} = \frac{1}{\sqrt{2}}(A_x + A_y).$$

If we know that the $x$-polarized mode is occupied by a photon, and the $y$-polarized mode is empty, what can be said about the possibility of finding a photon polarized along the $x'$ direction? This question is addressed in photon optics by invoking the usual probabilistic approach. The probabilities of finding a photon with $x$, $y$, $x'$, or $y'$ polarization are proportional to the intensities $|A_x|^2$, $|A_y|^2$, $|A_{x'}|^2$, and $|A_{y'}|^2$, respectively. In our example $|A_x|^2 = 1$, $|A_y|^2 = 0$, so that $|A_{x'}|^2 = |A_{y'}|^2 = \frac{1}{2}$. Therefore, given that there is one photon polarized along the $x$ direction and no photon polarized along the $y$ direction, the probabilities of finding a photon polarized along the $x'$ or $y'$ directions are both $\frac{1}{2}$. This is illustrated schematically in Fig. 11.1-4.

**EXAMPLE 11.1-1.** ***Transmission of a Linearly Polarized Photon Through a Polarizer.*** Consider a plane wave, linearly polarized at an angle $\theta$ with respect to the $x$ axis, directed onto a polarizer which has its transmission axis along the $x$ direction (see Fig. 11.1-5). The polarizer transmits light that is linearly polarized in the $x$ direction but blocks light that is linearly polarized in the $y$ direction. It is known from classical polarization optics that the intensity of the transmitted light $I_t = I_i\cos^2\theta$, where $I_i$ is the intensity of the incident light (see Sec. 6.1B). What happens if only a single photon impinges on the polarizer? If the photon is polarized along the $x$ axis, it always passes through. If it is



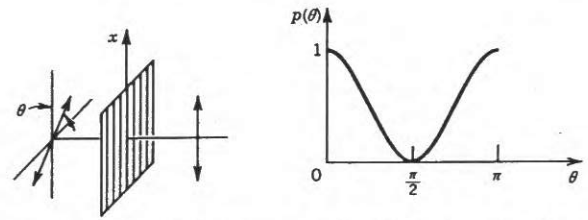


**Figure 11.1-5** Probability of observing a linearly polarized photon after transmission through a polarizer at an angle $\theta$.

polarized along the $y$ axis, it is always blocked. The probability for the passage of the photon is determined by the classical intensity $I_t$. Thus the probability of passage of a photon polarized at an angle $\theta$ with the polarizer is $p(\theta) = \cos^2\theta$. The probability that the photon is blocked is therefore $1 - p(\theta) = \sin^2\theta$.

### *Circularly Polarized Photons*

A modal expansion in terms of two circularly polarized plane-wave modes, one right-handed and one left-handed, can also be used, i.e.,

$$\mathbf{E}(\mathbf{r},t) = [A_R\hat{\mathbf{e}}_R + A_L\hat{\mathbf{e}}_L]\exp(-jkz)\exp(j2\pi\nu t),$$

where $\hat{\mathbf{e}}_R = (1/\sqrt{2})(\hat{\mathbf{x}} + j\hat{\mathbf{y}})$ and $\hat{\mathbf{e}}_L = (1/\sqrt{2})(\hat{\mathbf{x}} - j\hat{\mathbf{y}})$ (see Sec. 6.1B). These modes carry right-handed and left-handed circularly polarized photons, respectively. Again, the probabilities of finding a photon with these polarizations are proportional to the intensities $|A_R|^2$ and $|A_L|^2$. As illustrated in Fig. 11.1-6, a linearly polarized photon is equivalent to the superposition of a right-handed and a left-handed circularly polarized photon, each with probability $\frac{1}{2}$. Conversely, when a circularly polarized photon is passed through a linear polarizer, the probability of detecting it is $\frac{1}{2}$.

### *Photon Spin*

Photons possess intrinsic angular momentum (spin). The magnitude of the **photon spin** is quantized to the two values

$$\boxed{S = \pm\hbar.} \qquad (11.1\text{-}8)$$

Photon Spin

Right-handed (left-handed) circularly polarized photons have their spin vector parallel (antiparallel) to their momentum vector. Linearly polarized photons have an equal

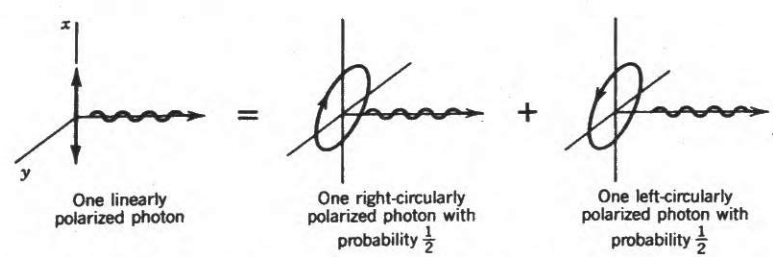


**Figure 11.1-6** A linearly polarized photon is equivalent to the superposition of a right- and left-circularly polarized photon, each with probability $\frac{1}{2}$.

probability of exhibiting parallel and antiparallel spin. In the same way that photons can transfer linear momentum to an object, circularly polarized photons can exert a torque on an object. For example, a circularly polarized photon will exert a torque on a half-wave plate of quartz.

## E. Photon Interference

Young's two-pinhole interference experiment is generally invoked to demonstrate the wave nature of light (see Exercise 2.5-2 on page 67). However, Young's experiment can be carried out even when there is only a single photon in the apparatus at a given time. The outcome of this experiment can be understood in the context of photon optics by using the photon-position rule. The intensity at the observation plane is calculated using electromagnetic (wave) optics and the result is converted to a probability density function that specifies the random position of the detected photon. The interference arises from phase differences in the two paths.

Consider a plane wave illuminating a screen with two pinholes, as shown in Fig. 11.1-7. This generates two spherical waves that interfere at the observation plane. In the Fresnel approximation these produce a sinusoidal intensity given by (see Exercise 2.5-2)

$$I(x) = 2I_0\left(1 + \cos\frac{2\pi\theta x}{\lambda}\right), \qquad (11.1\text{-}9)$$

where $I_0$ is the intensity of each of the waves at the observation plane, $\lambda$ is the wavelength, and $\theta$ is the angle subtended by the two pinholes at the observation plane (Fig. 11.1-7). The line that joins the holes defines the $x$ axis. The result in (11.1-9) describes the intensity pattern that is experimentally observed when the incident light is strong.

Now if only a single photon is present in the apparatus, the probability of detecting it at position $x$ is proportional to $I(x)$, in accordance with (11.1-5). It is most likely to be detected at those values of $x$ for which $I(x)$ is maximum. It will never be detected at values for which $I(x) = 0$. If a histogram of the locations of the detected photon is constructed by repeating the experiment many times, as Taylor did in 1909, the classical interference pattern obtained by carrying out the experiment once with a strong beam of light emerges. The interference pattern represents the probability distribution of the position at which the photon is observed.

The occurrence of interference results from the extended nature of the photon, which permits it to pass through *both* holes of the apparatus. This gives it knowledge of the entire geometry of the experiment when it reaches the observation plane, where it

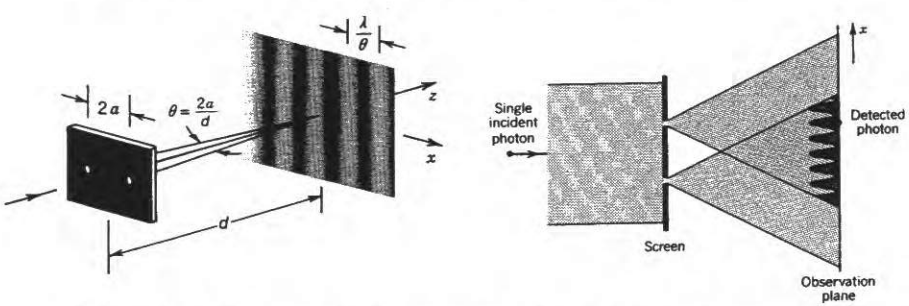


**Figure 11.1-7** Young's two-pinhole experiment with a single photon. The interference pattern $I(x)$ is proportional to the probability density of detecting the photon at position $x$.



is detected as a single entity. If one of the holes were to be covered, the interference pattern would disappear because the photon was forced to pass through the other hole, depriving it of knowledge of the whole apparatus.

### *EXERCISE 11.1-3*

***Photon in a Mach–Zehnder Interferometer.*** Consider a plane wave of light of wavelength $\lambda$ that is split into two parts at a beamsplitter (see Sec. 11.1B) and recombined in a Mach–Zehnder interferometer, as shown in Fig. 11.1-8 [see also Fig. 2.5-3(*a*)].

If the wave contains only a single photon, plot the probability of finding the photon at the detector as a function of $d/\lambda$ (for $0 \le d/\lambda \le 1$), where $d$ is the difference between the two optical paths of the light. Assume that the mirrors and beamsplitters are perfectly flat and lossless, and that the beamsplitters have a 50% reflectance. Where might the photon be located when the probability of finding it at the detector is not unity?

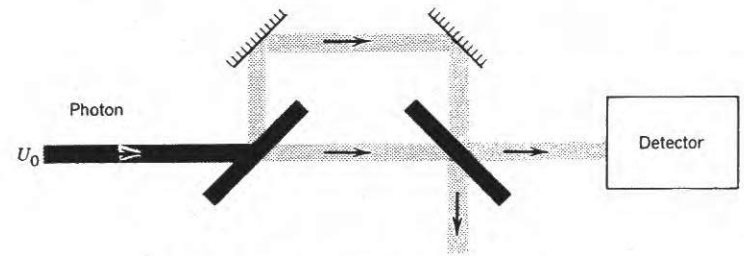


**Figure 11.1-8** Mach–Zehnder interferometer.

## F. Photon Time

The modal expansion provided in (11.1-1) represents monochromatic (single-frequency) modes which are "eternal" harmonic functions of time. A photon in a monochromatic mode is equally likely to be detected at any time. However, as indicated previously, a modal expansion of the radiation inside (or outside) a resonator is not unique. A more general expansion may be made in terms of polychromatic modes (time-localized wavepackets, for example). The probability of detecting the photon described by the complex wavefunction $U(\mathbf{r}, t)$ (see Sec. 2.6A) at any position, in the incremental time interval between $t$ and $t + dt$, is proportional to $I(\mathbf{r}, t)\,dt \propto |U(\mathbf{r}, t)|^2\,dt$.

The photon-position rule presented in (11.1-5) may therefore be generalized to include photon time localization:

**The probability of observing a photon at a point $\mathbf{r}$ within the incremental area $dA$, and during the incremental time interval $dt$ following time $t$, is proportional to the intensity of the mode at $\mathbf{r}$ and $t$, i.e.,**

$$p(\mathbf{r}, t)\,dA\,dt \propto I(\mathbf{r}, t)\,dA\,dt \propto |U(\mathbf{r}, t)|^2\,dA\,dt \qquad (11.1\text{-}10)$$

**Photon Position and Time**

### *Time–Energy Uncertainty*

The time during which a photon in a monochromatic mode of frequency $\nu$ may be detected is totally uncertain, whereas the value of its frequency $\nu$ (and its energy $h\nu$) is absolutely certain. On the other hand, a photon in a wavepacket mode with an intensity function $I(t)$ of duration $\sigma_t$ must be localized within this time. Bounding the photon time in this way engenders an uncertainty in the photon's frequency (and energy) as a result of the properties of the Fourier transform. The result is a "polychromatic" photon. The frequency uncertainty is readily determined by Fourier expanding $U(t)$ in terms of its harmonic components,

$$U(t) = \int_{-\infty}^{\infty} V(\nu) \exp(j2\pi\nu t)\, d\nu \tag{11.1-11}$$

where $V(\nu)$ is the Fourier transform of $U(t)$ (see Sec. A.1, Appendix A). The $\mathbf{r}$ dependence has been suppressed for simplicity. The width $\sigma_\nu$ of $|V(\nu)|^2$ represents the spectral width. If $\sigma_t$ is the rms width of the function $|U(t)|^2$ (i.e., the power-rms width), then $\sigma_t$ and $\sigma_\nu$ must satisfy the duration–bandwidth reciprocity relation $\sigma_\nu\sigma_t \geq 1/4\pi$, or $\sigma_\omega\sigma_t \geq \frac{1}{2}$ (see Sec. A.2, Appendix A for the definitions of $\sigma_t$ and $\sigma_\nu$ that lead to this uncertainty relation).

The energy of the photon $h\nu$ then cannot be specified to an accuracy better than $\sigma_E = h\sigma_\nu$. It follows that the energy uncertainty of a photon, and the time during which it may be detected, must satisfy

$$\boxed{\sigma_E\sigma_t \geq \frac{\hbar}{2},} \tag{11.1-12}$$

Time–Energy Uncertainty

known as the **time–energy uncertainty relation**. This relation is analogous to that between position and wavenumber (momentum), which sets a limit on the precision with which the position and momentum of a photon can be simultaneously specified. The average energy $\bar{E}$ of this polychromatic photon is $\bar{E} = h\bar{\nu} = \hbar\bar{\omega}$.

To summarize: A monochromatic photon ($\sigma_\nu \to 0$) has an eternal duration within which it can be observed ($\sigma_t \to \infty$). In contrast, a photon associated with an optical wavepacket is localized in time and is therefore polychromatic with a corresponding energy uncertainty. Thus a wavepacket photon can be viewed as a confined traveling packet of energy.

### *EXERCISE 11.1-4*

***Single Photon in a Gaussian Wavepacket.*** Consider a plane-wave wavepacket (see Sec. 2.6A) containing a single photon traveling in the $z$ direction, with complex wavefunction

$$U(\mathbf{r}, t) = {}_a\left(t - \frac{z}{c}\right)$$

where

$${}_a(t) = \exp\left(-\frac{t^2}{4\tau^2}\right)\exp(j2\pi\nu_0 t).$$

(a) Show that the uncertainties in its time and $z$ position are $\sigma_t = \tau$ and $\sigma_z = c\sigma_t$, respectively.



(b) Show that the uncertainties in its energy and momentum satisfy the minimum uncertainty relations

$$\sigma_E\sigma_t = \frac{\hbar}{2} \tag{11.1-13}$$

$$\sigma_z\sigma_p = \frac{\hbar}{2}. \tag{11.1-14}$$

Equation (11.1-14) is the minimum-uncertainty limit of the **Heisenberg position-momentum uncertainty relation** [see (A.2-7) in Appendix A].

## Summary

Electromagnetic radiation may be described as a sum of modes, e.g., monochromatic uniform plane waves of the form

$$\mathbf{E}(\mathbf{r}, t) = \sum_{\mathbf{q}} A_{\mathbf{q}} \exp(-j\mathbf{k}_{\mathbf{q}}\cdot\mathbf{r}) \exp(j2\pi\nu_{\mathbf{q}} t)\mathbf{e}_{\mathbf{q}}.$$

Each plane wave has two orthogonal polarization states (e.g., vertical/horizontal-linearly polarized, right/left-circularly polarized, etc.) represented by the vectors $\mathbf{e}_{\mathbf{q}}$. When the energy of a mode is measured, the result is an integer (in general, random) number of energy quanta (photons). Each of the photons associated with the mode $\mathbf{q}$ has the following properties:

- Energy $E = h\nu_{\mathbf{q}}$.
- Momentum $\mathbf{p} = \hbar\mathbf{k}$.
- Spin $S = \pm\hbar$, if it is circularly polarized.
- The photon is equally likely to be found anywhere in space, and at any time, since the wavefunction of the mode is a monochromatic plane wave.

The choice of modes is not unique. A modal expansion in terms of nonmonochromatic (quasimonochromatic), nonplanar waves,

$$\mathbf{E}(\mathbf{r}, t) = \sum_{\mathbf{q}} A_{\mathbf{q}} U_{\mathbf{q}}(\mathbf{r}, t)\mathbf{e}_{\mathbf{q}},$$

is also possible. The photons associated with the mode $\mathbf{q}$ then have the following properties:

- Photon position and time are governed by the complex wavefunction $U_{\mathbf{q}}(\mathbf{r}, t)$. The probability of detecting a photon in the incremental time between $t$ and $t + dt$, in an incremental area $dA$ at position $\mathbf{r}$, is proportional to $|U_{\mathbf{q}}(\mathbf{r}, t)|^2\, dA\, dt$.
- If $U_{\mathbf{q}}(\mathbf{r}, t)$ has a finite time duration $\sigma_t$, i.e., if the photon is localized in time, then the photon energy $h\nu_{\mathbf{q}}$ has an uncertainty $h\sigma_\nu \geq h/4\pi\sigma_t$.
- If $U_{\mathbf{q}}(\mathbf{r}, t)$ has a finite spatial extent in the transverse ($z = 0$) plane, i.e., if the photon is localized in the $x$ direction, for example, then the direction of photon momentum is uncertain. The spread in photon momentum can be determined by analyzing $U_{\mathbf{q}}(\mathbf{r}, t)$ as a sum of plane waves, the wave with wavevector $\mathbf{k}$ corresponding to photon momentum $\hbar\mathbf{k}$. Localization of the photon in the transverse plane results in a spread of the uncertainty of the photon-momentum direction.

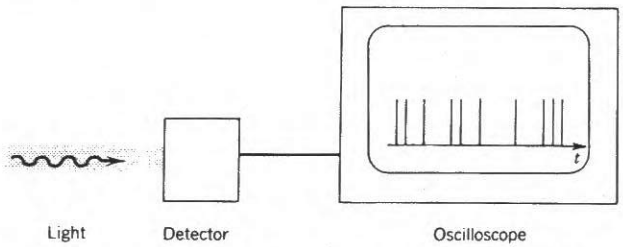


**Figure 11.2-1** Photon registrations at random localized instants of time.

## 11.2 PHOTON STREAMS

In Sec. 11.1 we concentrated on the properties and behavior of single photons. We now consider the properties of collections of photons. As a result of the processes by which photons are created (e.g., emissions from atoms; see Chap. 12), the number of photons occupying a mode is generally random. The probability distribution obeyed by the photon number is governed by the quantum state of the mode, which is determined by the nature of the light source (see Sec. 11.3). Real photon streams often contain numerous propagating modes, each carrying a random number of photons.

If an experiment is carried out in which a weak stream of photons falls on a light-sensitive surface, the photons are registered (detected) at random localized instants of time and at random points in space, in accordance with (11.1-10). This space–time process can be discerned by viewing an object with the naked eye in a dimly lit room.

The time course of such photon registrations can be highlighted by looking at the temporal and spatial behavior separately. Consider the use of a detector that integrates light over a finite area, as illustrated in Fig. 11.2-1. The probability of detecting a photon in the incremental time interval between $t$ and $t + dt$ is proportional to the optical power $P(t)$ at the time $t$. The photons will be registered at random times.

On the other hand, the spatial pattern of photon registrations is readily manifested by using a detector that integrates over a fixed exposure time $T$ (e.g., photographic film). In accordance with (11.1-10), the probability of observing a photon in an incremental area $dA$ surrounding the point $\mathbf{r}$ is proportional to the integrated local intensity $\int_0^T I(\mathbf{r}, t)\,dt$. This is illustrated by the "grainy" photographic image of Max Planck provided in Fig. 11.2-2. This image was obtained by rephotographing, under very low light conditions, the picture of Max Planck shown on page 384. Each of the white dots represents a random photon registration; the density of registrations follows the local intensity.

**Figure 11.2-2** Random photon registrations with a spatial density that follows the local optical intensity. This image of Max Planck taken with a weak stream of photons should be compared with the photograph on page 384 taken with intense light.



### A. Mean Photon Flux

We begin by introducing a number of definitions that relate the mean photon flux to classical electromagnetic intensity, power, and energy. These definitions are related to the probability law (11.1-10) governing the position and time at which a single photon is observed. We then discuss the randomness of the photon flux and the photon-number statistics for different sources of light. Finally, we consider the random partitioning of a photon stream.

#### *Mean Photon-Flux Density*

Monochromatic light of frequency $\nu$ and classical intensity $I(\mathbf{r})$ (watts/cm$^2$) carries a mean **photon-flux density**

$$\phi(\mathbf{r}) = \frac{I(\mathbf{r})}{h\nu}, \tag{11.2-1}$$

Mean Photon-Flux Density

where $h\nu$ is the energy of each photon. This equation converts a classical measure (with units of energy/s-cm$^2$) into a quantum measure (with units of photons/s-cm$^2$). For quasimonochromatic light of central frequency $\bar{\nu}$, all photons have approximately the same energy $h\bar{\nu}$, so that the mean photon-flux density is approximately

$$\phi(\mathbf{r}) = \frac{I(\mathbf{r})}{h\bar{\nu}}. \tag{11.2-2}$$

Typical values of $\phi(\mathbf{r})$ for some common sources of light are provided in Table 11.2-1. It is clear from these numbers that trillions of photons rain down on each square centimeter of us each second.

**TABLE 11.2-1 Mean Photon-Flux Density for Several Light Sources**

| Source | Mean Photon-Flux Density (photons/s-cm$^2$) |
|---|---|
| Starlight | $10^6$ |
| Moonlight | $10^8$ |
| Twilight | $10^{10}$ |
| Indoor light | $10^{12}$ |
| Sunlight | $10^{14}$ |
| Laser light (10-mW He–Ne laser beam at $\lambda_o = 633$ nm focused to a 20-$\mu$m-diameter spot) | $10^{22}$ |

### *Mean Photon Flux*

The mean photon flux $\Phi$ (with units of photons/s) is obtained by integrating the mean photon-flux density over a specified area,

$$\Phi = \int_A \phi(\mathbf{r})\, dA = \frac{P}{h\bar{\nu}}, \qquad \text{(11.2-3)}$$

Mean Photon Flux

where again $h\bar{\nu}$ is the average energy of a photon, and

$$P = \int_A I(\mathbf{r})\, dA \qquad \text{(11.2-4)}$$

is the optical power (watts). As an example, 1 nW of optical power, at a wavelength $\lambda_o = 0.2\ \mu$m, delivers to an object an average photon flux $\Phi \approx 10^9$ photons per second. Roughly speaking, one photon will therefore strike the object every nanosecond, i.e.,

$$\text{1 nW at } \lambda_o = 0.2\ \mu\text{m} \rightarrow \text{1 photon/ns.} \qquad \text{(11.2-5)}$$

A $\lambda_o = 1\ \mu$m photon carries one-fifth of the energy, so that 1 nW corresponds to an average of 5 photons/ns.

### *Mean Number of Photons*

The mean number of photons $\bar{n}$ detected in the area $A$ and the time interval $T$ is obtained by multiplying the photon flux $\Phi$ by the time duration,

$$\bar{n} = \Phi T = \frac{E}{h\bar{\nu}}, \qquad \text{(11.2-6)}$$

Mean Photon Number

where $E = PT$ is the optical energy (joules).

To summarize, the relations between the classical and quantum measures are:

| Classical | | Quantum | |
|---|---|---|---|
| Optical intensity | $I(\mathbf{r})$ | Photon-flux density | $\phi(\mathbf{r}) = \dfrac{I(\mathbf{r})}{h\bar{\nu}}$ |
| Optical power | $P$ | Photon flux | $\Phi = \dfrac{P}{h\bar{\nu}}$ |
| Optical energy | $E$ | Photon number | $\bar{n} = \dfrac{E}{h\bar{\nu}}$ |

### *Spectral Densities of Photon Flux*

For polychromatic light of broad bandwidth, it is useful to define spectral densities of the classical intensity, power, and energy, and their quantum counterparts: spectral photon-flux density, spectral photon flux, and spectral photon number:



| Classical | Quantum |
|---|---|
| $I_\nu$ (W/cm$^2$-Hz) | $\phi_\nu = \dfrac{I_\nu}{h\nu}$ (photons/s-cm$^2$-Hz) |
| $P_\nu$ (W/Hz) | $\Phi_\nu = \dfrac{P_\nu}{h\nu}$ (photons/s-Hz) |
| $E_\nu$ (J/Hz) | $\bar{n}_\nu = \dfrac{E_\nu}{h\nu}$ (photons/Hz) |

For example, $P_\nu\, d\nu$ represents the optical power in the frequency range $\nu$ to $\nu + d\nu$; and $\Phi_\nu\, d\nu$ represents the flux of photons whose frequency lies between $\nu$ and $\nu + d\nu$.

### *Time-Varying Light*

If the light intensity is time varying, the photon-flux density is a function of time,

$$\phi(\mathbf{r}, t) = \frac{I(\mathbf{r}, t)}{h\bar{\nu}}. \qquad \text{(11.2-7)}$$

The optical power and the photon flux are also, then, functions of time:

$$\Phi(t) = \int_A \phi(\mathbf{r}, t)\, dA = \frac{P(t)}{h\bar{\nu}}, \qquad \text{(11.2-8)}$$

Mean Photon Flux

where

$$P(t) = \int_A I(\mathbf{r}, t)\, dA. \qquad \text{(11.2-9)}$$

The mean number of photons registered in a time interval between $t = 0$ and $t = T$ also varies with time. It is obtained by integrating the photon flux,

$$\bar{n} = \int_0^T \Phi(t)\, dt = \frac{E}{h\bar{\nu}}, \qquad \text{(11.2-10)}$$

Mean Photon Number

where

$$E = \int_0^T P(t)\, dt = \int_0^T \int_A I(\mathbf{r}, t)\, dA\, dt. \qquad \text{(11.2-11)}$$

is the optical energy (the intensity integrated over time and area).

## B. Randomness of Photon Flux

Even if the classical intensity $I(\mathbf{r}, t)$ is constant, the time of arrival and position of registration of a single photon are governed by probabilistic laws, as we have seen in Sec. 11.1 (see Fig. 11.2-1). If a source provides exactly one photon, the probability density of detecting that photon at the space–time point $(\mathbf{r}, t)$ is proportional to $I(\mathbf{r}, t)$, in accordance with (11.1-10). We shall see in this section that the classical electromag-

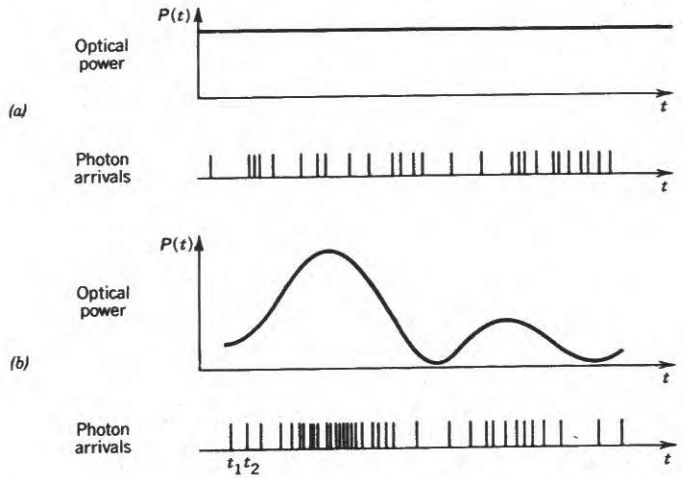


**Figure 11.2-3** (*a*) Constant optical power and the corresponding random photon arrival times. (*b*) Time-varying optical power and the corresponding random photon arrival times.

netic intensity $I(\mathbf{r}, t)$ governs the behavior of photon streams as well as single photons. The interpretation ascribed to $I(\mathbf{r}, t)$ differs, however. *For photon streams, the classical intensity $I(\mathbf{r}, t)$ determines the mean photon-flux density $\phi(\mathbf{r}, t)$. The properties of the light source determine the fluctuations in $\phi(\mathbf{r}, t)$.*

If the optical power $P(t)$ varies with time, the density of random times at which the associated photons are detected generally follows the function $P(t)$, as schematically illustrated in Fig. 11.2-3. The mean flux $\Phi(t)$ is $P(t)/h\bar{\nu}$, but the actual times at which the photons are detected are random. Where the power is large, there are, on the average, more photons; where the power is small, the photons are sparse. Even when $P$ is constant, the times at which the photons are detected is random, with behavior determined by the source (Figs. 11.2-3(*a*) and 11.2-4). For example, at $\lambda_o = 1.24\ \mu$m, 1 nW carries an *average* of 6.25 photons/ns, or 0.00625 photons every picosecond. Of course, only integral numbers of photons may be detected. An average of 0.00625 photons/ps means that if $10^5$ time intervals (each of duration $T = 1$ ps) were examined, most of the time intervals would be empty (no photons), about 625 intervals would contain one photon, and very few intervals would contain two or more photons.

The image of Max Planck in Fig. 11.2-2 shows the same behavior in the spatial domain. The locations of the detected photons generally follow the classical intensity distribution, with a high density of photons where the intensity is large and low photon density where the intensity is small. But there is considerable graininess (noise) in the image. Fluctuations in the photon-flux density are most discernible when its mean value is small, as in the case of Fig. 11.2-2. When the mean photon-flux density becomes large everywhere in the image, the graininess disappears and the classical intensity distribution is recovered, as seen in the picture of Max Planck on page 384.

The study of the randomness of photon numbers is important for applications such as noise in weak images and optical information transmission. In a fiber-optic communication system, for example, information is carried on a photon stream (see Sec. 22.3). Only the mean number of photons emitted by the source is controlled at the transmitter. The actual number of emitted photons is unpredictable, the nature of the source



determining the form of its randomness. The unpredictability of the photon number results in errors in the transmission of information.

## C. Photon-Number Statistics

The statistical distribution of the number of photons depends on the nature of the light source and must generally be treated by use of the quantum theory of light, as described briefly in Sec. 11.3. However, under certain conditions, the arrival of photons may be regarded as the independent occurrences of a sequence of random events at a rate equal to the photon flux, which is proportional to the optical power. The optical power may be deterministic (as in coherent light) or random (as in partially coherent light). For partially coherent light, the power fluctuations are correlated, so that the arrival of photons is no longer a sequence of independent events; the photon statistics are then significantly different.

### *Coherent Light*

Consider light of constant optical power $P$. The corresponding mean photon flux $\Phi = P/h\bar{\nu}$ (photons/s) is also constant, but the actual times of registration of the photons are random as shown in Fig. 11.2-4. Given a time interval of duration $T$, let the number of detected photons be $n$. We already know that the mean value of $n$ is $\bar{n} = \Phi T = PT/h\bar{\nu}$. We wish to obtain an expression for the probability distribution $p(n)$, i.e., the probability $p(0)$ of detecting no photons, the probability $p(1)$ of detecting one photon, and so on.

An expression for the probability distribution $p(n)$ can be derived under the assumption that the registrations of photons are statistically independent. The result is the Poisson distribution

$$p(n) = \frac{\bar{n}^n \exp(-\bar{n})}{n!}, \qquad n = 0, 1, 2, \ldots . \tag{11.2-12}$$

Poisson Distribution

This distribution, known as the **Poisson distribution**, is displayed on a semilogarithmic plot in Fig. 11.2-5 for several values of the mean $\bar{n}$. The curves become progressively broader as $\bar{n}$ increases.

### *Derivation of the Poisson Distribution*

Divide the time interval $T$ into a large number $N$ of subintervals of sufficiently small width $T/N$ each, such that each interval carries one photon with probability $p = \bar{n}/N$ and no photons with probability $1 - p$. The probability of finding $n$ independent


**Figure 11.2-4** Random arrival of photons in a light beam of power $P$ within intervals of duration $T$. Although the optical power is constant, the number $n$ of photons arriving within each interval is random.

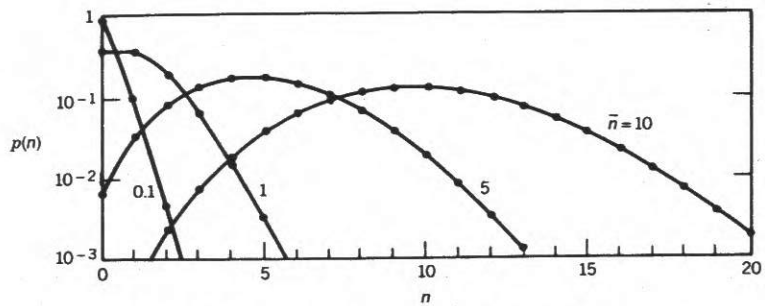


**Figure 11.2-5** Poisson distribution $p(n)$ of the photon number $n$.

photons in the $N$ intervals, like the flips of a biased coin, then follows the binomial distribution

$$p(n) = \frac{N!}{n!\,(N-n)!}p^n(1-p)^{N-n},$$

$$= \frac{N!}{n!\,(N-n)!}\left(\frac{\bar{n}}{N}\right)^n\left(1-\frac{\bar{n}}{N}\right)^{N-n}.$$

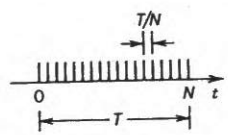


In the limit as $N \to \infty$, $N!/(N-n)!\,N^n \to 1$, and $[1-(\bar{n}/N)]^{N-n} \to \exp(-\bar{n})$, so that (11.2-12) is obtained.

### *Mean and Variance*

Two important parameters characterize any random number $n$—its mean value,

$$\bar{n} = \sum_{n=0}^{\infty} np(n), \tag{11.2-13}$$

and its variance

$$\sigma_n^2 = \sum_{n=0}^{\infty} (n-\bar{n})^2 p(n), \tag{11.2-14}$$

which is the average of the squared deviation from the mean. The standard deviation $\sigma_n$ (the square root of the variance) is a measure of the width of the distribution. The quantities $p(n)$, $\bar{n}$, and $\sigma_n$ are collectively called the photon-number statistics. Although the function $p(n)$ contains more information than just its mean and variance, these are useful measures.

It is not difficult to show [by use of (11.2-12) in (11.2-13) and (11.2-14)] that the mean of the Poisson distribution is indeed $\bar{n}$ and its variance is equal to its mean,

$$\boxed{\sigma_n^2 = \bar{n}.} \tag{11.2-15}$$

Variance of the Poisson Distribution



For example, when $\bar{n} = 100$, $\sigma_n = 10$; i.e., the generation of 100 photons is accompanied by an inaccuracy of about $\pm 10$ photons.

The Poisson photon-number distribution applies for many light sources, including an ideal laser emitting a beam of monochromatic coherent light in a single mode (see Chap. 14). This distribution corresponds to a quantum state of light known as the coherent state (see Sec. 11.3A).

### *Signal-to-Noise Ratio*

The randomness of the number of photons constitutes a fundamental source of noise that we have to contend with when using light to transmit a signal. Representing the mean of the signal as $\bar{n}$ and its noise by the root mean square value $\sigma_n$, a useful measure of the performance of light as an information-carrying medium is the signal-to-noise ratio (SNR). The SNR of the random number $n$ is defined as

$$\text{SNR} \equiv \frac{(\text{mean})^2}{\text{variance}} = \frac{\bar{n}^2}{\sigma_n^2}. \tag{11.2-16}$$

For the Poisson distribution

$$\boxed{\text{SNR} = \bar{n},} \tag{11.2-17}$$

Poisson Photon-Number Signal-to-Noise Ratio

i.e., the signal-to-noise ratio increases without limit as the mean photon number increases.

Although the SNR is a useful measure of the randomness of a signal, in some applications it is necessary to know the probability distribution itself. For example, if one communicates by sending a mean number of photons $\bar{n} = 20$, according to (11.2-12) the probability that no photons are received is $p(0) \approx 2 \times 10^{-9}$. This represents a probability of error in the transmission of information. This topic is addressed in Chap. 22.

### *Thermal Light*

When the photon arrival times are correlated, the photon number statistics obey distributions other than the Poisson. This is the case for thermal light. Consider an optical resonator whose walls are maintained at temperature $T$ kelvins (K), so that photons are emitted into the modes of the resonator. In accordance with the laws of statistical mechanics, under conditions of thermal equilibrium the probability distribution for the electromagnetic energy $E_n$ in one of its modes satisfies the **Boltzmann probability distribution**

$$\boxed{P(E_n) \propto \exp\left(-\frac{E_n}{k_B T}\right).} \tag{11.2-18}$$

Boltzmann Distribution

Here $k_B$ is **Boltzmann's constant** ($k_B = 1.38 \times 10^{-23}$ J/K). The energy associated with each mode is random. Higher energies are relatively less probable than lower energies, in accordance with a simple exponential law governed by the quantity $k_B T$. The smaller the value of $k_B T$, the less likely are higher energies. At room temperature ($T = 300$ K), $k_B T = 0.026$ eV, which is equivalent to 208 $\text{cm}^{-1}$. The Boltzmann

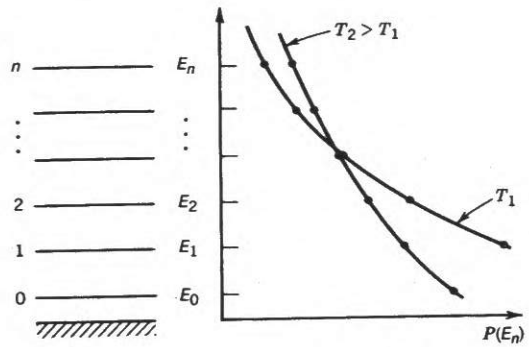


**Figure 11.2-6** Boltzmann probability distribution $P(E_n)$ versus energy $E_n$.

distribution for this single mode is sketched in Fig. 11.2-6 with temperature as a parameter.

It follows from (11.2-18) and the photon-energy quantization relation given by $E_n = (n + \frac{1}{2})h\nu$ that the probability of finding $n$ photons in a single mode of a resonator in thermal equilibrium is given by

$$p(n) \propto \exp\left(-\frac{nh\nu}{k_B T}\right)$$

$$= \left[\exp\left(-\frac{h\nu}{k_B T}\right)\right]^n, \qquad n = 0, 1, 2, \ldots . \tag{11.2-19}$$

Using the condition that the probability distribution must have a sum equal to unity, i.e., $\sum_{n=0}^{\infty} p(n) = 1$, the normalization constant is determined to be $[1 - \exp(-h\nu/k_B T)]$. The zero-point energy $E_0 = \frac{1}{2}h\nu$ disappears into the normalization and does not affect the results, in accordance with the discussion in Sec. 11.1A.

The result is most simply written in terms of its mean $\bar{n}$ as

$$\boxed{p(n) = \frac{1}{\bar{n} + 1}\left(\frac{\bar{n}}{\bar{n} + 1}\right)^n,} \tag{11.2-20}$$

Bose–Einstein Distribution

where

$$\bar{n} = \frac{1}{\exp(h\nu/k_B T) - 1}, \tag{11.2-21}$$

as determined from (11.2-13). In the parlance of probability theory, this distribution is called the **geometric distribution** since $p(n)$ is a geometrically decreasing function of $n$. In physics it is referred to as the **Bose–Einstein probability distribution.**

The Bose–Einstein distribution is displayed on a semilogarithmic plot in Fig. 11.2-7, for several values of $\bar{n}$ (or equivalently, for several values of the temperature $T$). Its exponential character is evident in the straight-line behavior in the plot. Comparing



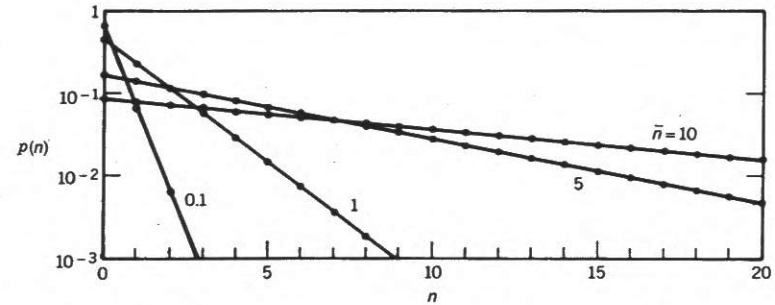


**Figure 11.2-7** Bose–Einstein distribution $p(n)$ of the photon number $n$.

Figs. 11.2-7 with 11.2-5 demonstrates that the photon-number distribution for thermal light is far broader than that for coherent light.

Using (11.2-14), the photon-number variance turns out to be

$$\boxed{\sigma_n^2 = \bar{n} + \bar{n}^2.} \tag{11.2-22}$$

Bose–Einstein Variance

Comparing this expression to the variance for the Poisson distribution, which is simply $\bar{n}$, we see that thermal light has a larger variance corresponding to more uncertainty and a greater range of fluctuations of the photon number. The signal-to-noise ratio of the Bose–Einstein distribution is

$$\text{SNR} = \frac{\bar{n}}{\bar{n} + 1};$$

it is always smaller than unity no matter how large the optical power. The amplitude and phase of thermal light behave like random quantities, as described in Chapter 10. This randomness results in a broadening of the photon-number distribution. Indeed, this form of light is too noisy to be used in high-data-rate information transmission.

### *EXERCISE 11.2-1*

***Average Energy in a Resonator Mode.*** Show that the average energy of a resonator mode of frequency $\nu$, under conditions of thermal equilibrium at temperature $T$, is given by

$$\bar{E} = k_B T \frac{h\nu/k_B T}{\exp(h\nu/k_B T) - 1}. \tag{11.2-23}$$

Sketch the dependence of $\bar{E}$ on $\nu$ for several values of $k_B T/h$. Use a Taylor series expansion of the denominator to obtain a simplified approximate expression for $\bar{E}$ in the limit $h\nu/k_B T \ll 1$. Explain the result on a physical basis.

### *Other Sources of Light

As mentioned earlier, for a certain class of light sources the photon arrivals can be regarded as a sequence of independent events, arriving at a rate proportional to the optical power. For coherent light, the power is deterministic, and the photon number obeys the Poisson distribution $p(n) = \mathscr{W}^n e^{-\mathscr{W}}/n!$, where

$$\mathscr{W} = \frac{1}{h\nu}\int_0^T P(t)\,dt = \frac{1}{h\nu}\int_0^T\int_A I(\mathbf{r},t)\,dA\,dt. \tag{11.2-24}$$

The integrated optical power normalized to units of photon number, $\mathscr{W}$, is a constant representing the mean photon number $\bar{n}$.

When the intensity $I(\mathbf{r}, t)$ itself fluctuates randomly in time and/or space, the optical power $P(t)$ also undergoes random fluctuations [see Fig. 11.2-3(*b*)], and its integral $\mathscr{W}$ is therefore also random. As a result, not only is the photon number random but so is its mean $\mathscr{W}$. Because of this added source of randomness, the photon-number statistics for partially coherent light will differ from the Poisson distribution. If the fluctuations in the mean photon number $\mathscr{W}$ are described by a probability density function $p(\mathscr{W})$, the unconditional probability distribution for partially coherent light may be obtained by averaging the conditional Poisson distribution $p(n|\mathscr{W}) = \mathscr{W}^n e^{-\mathscr{W}}/n!$ over all permitted values of $\mathscr{W}$, each weighted by its probability density $p(\mathscr{W})$. The resultant photon-number distribution is then

$$\boxed{p(n) = \int_0^\infty \frac{\mathscr{W}^n e^{-\mathscr{W}}}{n!} p(\mathscr{W})\,d\mathscr{W},} \tag{11.2-25}$$

Mandel's Formula

which is known as Mandel's formula. Equation (11.2-25) is also referred to as the doubly stochastic Poisson counting distribution because of the two sources of randomness that contribute to it: the photons themselves (which behave in Poisson fashion) and the intensity fluctuations arising from the noncoherent nature of the light (which must be specified).

Note that this theory of photon statistics is applicable only to a certain class of light (called classical light); a more general theory based on a quantum description of the state of light is described briefly in Sec. 11.3.

The photon-number mean and variance for partially coherent light, which can be derived by using (11.2-13) and (11.2-14) in conjunction with (11.2-25), are

$$\bar{n} = \overline{\mathscr{W}} \tag{11.2-26}$$

and

$$\sigma_n^2 = \bar{n} + \sigma_{\mathscr{W}}^2, \tag{11.2-27}$$

respectively. Here $\sigma_{\mathscr{W}}^2$ signifies the variance of $\mathscr{W}$. Note that the variance of the photon number is the sum of two contributions—the first term is the basic contribution of the Poisson distribution, and the second is an additional contribution due to the classical fluctuations of the optical power.



In one important example of statistical fluctuations, the normalized integrated optical power $\mathscr{W}$ obeys the exponential probability density function

$$p(\mathscr{W}) = \begin{cases} \frac{1}{\overline{\mathscr{W}}}\exp\left(-\frac{\mathscr{W}}{\overline{\mathscr{W}}}\right), & \mathscr{W} \geq 0 \\ 0, & \mathscr{W} < 0. \end{cases} \tag{11.2-28}$$

This distribution is applicable to quasi-monochromatic spatially coherent light, when the real and imaginary components of the complex amplitude are independent and have normal (Gaussian) probability distributions. The spectral width must be sufficiently small so that the coherence time $\tau_c$ is much greater than the counting time $T$, and the coherence area $A_c$ must be much larger than the area of the detector $A$. The photon-number distribution $p(n)$ corresponding to (11.2-28) can be obtained by substitution into (11.2-25) and evaluation of the integral. The result turns out to be the Bose–Einstein distribution given in (11.2-20). The Gaussian-distributed optical field therefore has photon statistics identical to those of single-mode thermal light. When the area $A$ and the time $T$ are not small, the statistics are modified; they describe multimode thermal light (see Probs. 11.2-5 to 11.2-7).

## D. Random Partitioning of Photon Streams

A photon stream is said to be partitioned when it is subjected to the removal of some of its photons. The photons removed may be either diverted or destroyed. The process is called random partitioning when they are diverted and random deletion when they are destroyed. There are numerous ways in which this can occur. Perhaps the simplest example of random partitioning is provided by an ideal lossless beamsplitter. Photons are randomly selected to join either of the two emerging streams (see Fig. 11.2-8). An example of random deletion is provided by the action of an optical absorption filter on a light beam. Photons are randomly selected either to pass through the filter or to be destroyed (and converted into heat).

We restrict our treatment to situations in which the possibility of each photon being removed behaves in accordance with an independent random (Bernoulli) trial. In terms of the beamsplitter, this is satisfied if a photon stream impinges on only one of the input ports (Fig. 11.2-8). This eliminates the possibility of interference, which, in general, invalidates the independent-trial assumption. Although the results derived below are couched in terms of random partitioning, they apply equally well to random deletion.

Consider a lossless beamsplitter with transmittance $\mathscr{T}$ and reflectance $\mathscr{R} = 1 - \mathscr{T}$. In electromagnetic optics, the intensity of the transmitted wave $I_t$ is related to the intensity of the incident wave $I$ by $I_t = \mathscr{T}I$. The result of a single photon impinging on a beamsplitter was examined in Sec. 11.1B; it was shown that the probability of transmission is equal to the transmittance $\mathscr{T}$. We now proceed to calculate the

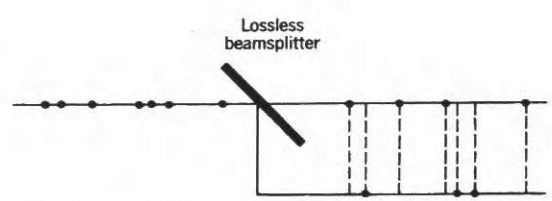


**Figure 11.2-8** Random partitioning of photons by a beamsplitter.

outcome when a photon stream of mean flux $\Phi$ is incident, so that a mean number of photons $\bar{n} = \Phi T$ strikes the beamsplitter in the time interval $T$.

In accordance with (11.2-6), the mean number of photons in a beam is proportional to the optical energy. The mean number of transmitted and reflected photons in this time must therefore be $\mathscr{T}\bar{n}$ and $(1 - \mathscr{T})\bar{n}$, respectively. We now consider a more general question: what happens to the photon-number statistics $p(n)$ of the photon stream on partitioning by a beamsplitter?

A single photon falling on the beamsplitter is transmitted with probability $\mathscr{T}$ and reflected with probability $1 - \mathscr{T}$ (see Fig. 11.1-3). If the incident beam contains precisely $n$ photons, the probability $p(m)$ that $m$ photons are transmitted is the same as that of flipping a coin $n$ times, where the probability of achieving a head (being transmitted) is $\mathscr{T}$. From elementary probability theory we know that the outcome is the binomial distribution

$$p(m) = \binom{n}{m}\mathscr{T}^m(1 - \mathscr{T})^{n-m}, \qquad m = 0, 1, \ldots, n, \tag{11.2-29}$$

where $\binom{n}{m} = n!/m!(n - m)!$. The mean number of transmitted photons is easily shown to be

$$\bar{m} = \mathscr{T}n. \tag{11.2-30}$$

The variance for the binomial distribution is given by

$$\sigma_m^2 = \mathscr{T}(1 - \mathscr{T})n = (1 - \mathscr{T})\bar{m}. \tag{11.2-31}$$

Because of the symmetry of the problem, the results for the reflected beam are obtained immediately. As the average number of transmitted photons $\bar{m}$ increases, the signal-to-noise ratio, represented by $\bar{m}^2/\sigma_m^2 = \bar{m}/(1 - \mathscr{T})$ increases. Therefore, for large intensities, the photons will be partitioned between the two streams in good accord with $\mathscr{T}$ and $(1 - \mathscr{T})$, indicating that the laws of classical optics are recovered.

The expressions provided above are useful because they permit us to calculate the effect of a beamsplitter on photons obeying various photon-number statistics. The solution is obtained by recognizing that in these cases the number of photons $n$ at the input to the beamsplitter is random rather than fixed. Let the probability that there are exactly $n$ photons present be $p_0(n)$. If we treat the photons as independent events, the photon-number probability distribution in the transmitted stream will be a weighted sum of binomial distributions, with $n$ taking on the random value $n$. The weighting is in accordance with the probability that $n$ photons were present. The probability of finding $m$ photons transmitted through the beamsplitter, when the input photon-number distribution is $p_0(n)$, is therefore given by $p(m) = \sum_n p(m|n)p_0(n)$, where $p(m|n) = \binom{n}{m}\mathscr{T}^m(1 - \mathscr{T})^{n-m}$ is the binomial distribution. Explicitly, then,

$$p(m) = \sum_{n=m}^{\infty} \binom{n}{m}\mathscr{T}^m(1 - \mathscr{T})^{n-m}p_0(n), \qquad m = 0, 1, 2, \ldots. \tag{11.2-32}$$

Photon-Number Statistics under Random Partitioning

When $p_0(n)$ is the Poisson distribution (coherent light) or the Bose–Einstein distribution (thermal light), the results turn out to be quite simple: $p(m)$ has exactly the same form of photon-number distribution as $p_0(n)$. These distributions retain their form under random partitioning. Thus single-mode laser light transmitted through a beamsplitter remains Poisson and thermal light remains Bose–Einstein, but of course



with a reduced photon-number mean. Light with a deterministic number of photons (see Sec. 11.3B), on the other hand, does not retain its form under random partitioning, and this unfortunate property accounts for its lack of robustness.

The signal-to-noise ratio of $m$ is easily calculated for photon streams that have undergone partitioning or deletion. For coherent light and single-mode thermal light, the results are

$$\text{SNR} = \begin{cases} \mathscr{T}\bar{n} & \text{coherent light} \qquad (11.2\text{-}33) \\ \dfrac{\mathscr{T}\bar{n}}{\mathscr{T}\bar{n} + 1} & \text{thermal light.} \qquad (11.2\text{-}34) \end{cases}$$

Since $\mathscr{T} \leq 1$ it is clear that random partitioning decreases the signal-to-noise ratio. Another way of stating this is that random partitioning introduces noise. The effect is most severe for deterministic photon-number light.

The same results are also applicable to the *detection* of photons. If every photon has an independent chance of being detected, then out of $n$ incident photons, $m$ photons would be detected where $p(m)$ is related to $p_0(n)$ by (11.2-32). This result will be useful in the theory of photon detection (Chap. 17).

## *11.3 QUANTUM STATES OF LIGHT

The position, momentum, and number of photons in an electromagnetic mode are generally random quantities. In this section it will be shown that the electric field itself is also generally random. Consider a plane-wave monochromatic electromagnetic mode in a volume $V$, described by the electric field $\text{Re}\{\mathbf{E}(\mathbf{r}, t)\}$, where

$$\mathbf{E}(\mathbf{r}, t) = A \exp(-j\mathbf{k} \cdot \mathbf{r}) \exp(j2\pi\nu t)\hat{\mathbf{e}}.$$

According to classical electromagnetic optics, the energy of the mode is fixed at $\frac{1}{2}\epsilon|A|^2V$. We define a complex variable $a$, such that $\frac{1}{2}\epsilon|A|^2V = h\nu|a|^2$, which allows $|a|^2$ to be interpreted as the energy of the mode in units of photon number. The electric field may then be written as

$$\mathbf{E}(\mathbf{r}, t) = \left(\frac{2h\nu}{\epsilon V}\right)^{1/2} a \exp(-j\mathbf{k} \cdot \mathbf{r}) \exp(j2\pi\nu t)\hat{\mathbf{e}}, \tag{11.3-1}$$

where the complex variable $a$ determines the complex amplitude of the field.

In classical electromagnetic optics, $a \exp(j2\pi\nu t)$ is a rotating phasor whose projection on the real axis determines the sinusoidal electric field (see Fig. 11.3-1). The real and imaginary parts $x = \text{Re}\{a\}$ and $p = \text{Im}\{a\}$ are called the quadrature components of the phasor $a$ because they are a quarter cycle (90°) out of phase with each other. They determine the amplitude and phase of the sine wave that represents the temporal variation of the electric field. The rotating phasor $a \exp(j2\pi\nu t)$ also describes the motion of a harmonic oscillator; the real component $x$ is proportional to position and the imaginary component $p$ to momentum. From a mathematical point of view, a classical monochromatic mode of the electromagnetic field and a classical harmonic oscillator behave identically.

Similarly, a quantum monochromatic electromagnetic mode and a one-dimensional quantum-mechanical harmonic oscillator have identical behavior. We therefore review the quantum theory of a simple harmonic oscillator before proceeding.